Table II. Clinical profile at admission

Variable	n (%)
No. of patients	1100
New York Heart Association functional class	
I	8 (0.7)
II	134 (12.1)
III	434 (39.1)
IV	524 (47.2)
Physical findings	
Paroxysmal nocturnal dyspnea	615 (55.4)
Orthopnea	760 (68.5)
Rales	861 (77.6)
Third heart sound	449 (40.5)
Jugular venous distension	680 (61.3)
Peripheral edema	752 (67.7)
Cold extremities	259 (23.3)
Noninvasive hemodynamic assessments	
Warm & dry	44 (4.0)
Warm & wet	818 (73.7)
Cold & dry	30 (2.7)
Cold & wet	188 (16.9)

Table III. In-hospital management

Variable	n (%)
No. of patients	1100
Intravenous drugs	
Diuretics	894 (80.4)
Carperitide	770 (69.4)
Isosorbide dinitrate	102 (9.2)
Nitroglycerin	289 (26.0)
Nicorandil	118 (10.6)
Inotropes, any	230 (20.7)
Dobutamine	141 (12.7)
Dopamine	122 (11.0)
Norepinephrine	69 (6.2)
Milrinone	31 (2.8)
Olprinone	8 (0.7)
Digoxin	72 (6.5)
Calcium-channel blocker	91 (8.2)
Nonpharmacologic managements	
Continuous positive airway pressure	241 (21.7)
Bilevel positive airway pressure	160 (14.4)
Intubation	123 (11.1)
Swan-Ganz catheter	223 (20.1)
Pacemaker	52 (4.7)
Cardiac resynchronization therapy	27 (2.4)
Implantable cardioverter-defibrillator	29 (2.6)
Hemodialysis	39 (3.5)
Continuous hemodiafiltration	41 (3.7)
Percutaneous coronary intervention	107 (9.6)
Coronary artery bypass grafting	15 (1.4)
Valve replacement	19 (1.7)
Intraaortic balloon pump	40 (3.6)
Percutaneous cardiopulmonary support	7 (0.6)
Left ventricular assist system	1 (0.1)

and mortality is examined as follows: (1) readmission for heart failure; (2) death from heart failure; (3) sudden death; (4) death from other cardiac causes; (5) death from cerebral or vascular causes; (6) death from a noncardiac, cerebral, or vascular cause; and (7) idiopathic death. Hospital and 30-day mortality are evaluated using composite and component end points. Medium-term morbidity and mortality is also examined for the same components as for short-term morbidity and mortality. Sixty-, 90-, and 180-day morbidity and mortality are estimated by the Kaplan-Meier method using the dates of admission and discharge as observation start points. Short- and medium-term morbidity and mortality data are obtained and updated by the attending physicians in the ATTEND Web database at the appropriate times. Thus, the present report provides information about the demographic characteristics, clinical profile, management, and in-hospital mortality, whereas further data will be reported once the database is closed at the end of study.

This study is being conducted based on the Helsinki Declaration and the Japanese Ethical Guidelines for Clinical Studies. During the planning, implementation and reporting of this study, there were no issues such as conflict of interest, conflict of responsibility, or intellectual property rights. The present study does not affect patient rights.

Funding, creation of the paper, and conflict of interest

The present study is funded by the Japan Heart Foundation. The authors are responsible for the design and conduct of this study, the drafting and editing of the present article, and its final content. All analyses were performed at an independent biostatistics and data center (STATZ Institute, Inc, Tokyo, Japan). All authors have no disclosures.

Statistical analysis

Descriptive statistics were calculated based on clinical characteristics and treatment information for the registered patients. When continuous variables were assumed to show a normal distribution, the data were expressed as the mean ± SD. When normality was not assumed, the data were expressed as the median with interquartile range. Categorical data were summarized as the frequency and proportion. The 95% CIs of the mean, median, and proportion values were also estimated.

Results

Clinical profile of AHFS in the present study and comparison to those of Western studies

As of May 18, 2009, a total of 1,110 patients had been enrolled at 29 hospitals. The characteristics of these patients are shown in Table I. The mean age was 73 ± 14 years and 58.9% were men. The percentage of patients with a history of hospitalization for heart failure was lower than that of patients with de novo heart failure (37.4% vs 62.6%). Hypertension was the most common risk factor (70.6%). The underlying diseases that led to AHFS were ischemic heart disease in 33.2%, hypertensive heart disease in 18.4%, dilated cardiomyopathy in 12.7%, and valvular disease in 17.3%.

The demographic characteristics and prevalence of comorbidities were broadly comparable with those in Western countries, except for chronic obstructive pulmonary disease. Ischemic etiology was relatively

Figure 2

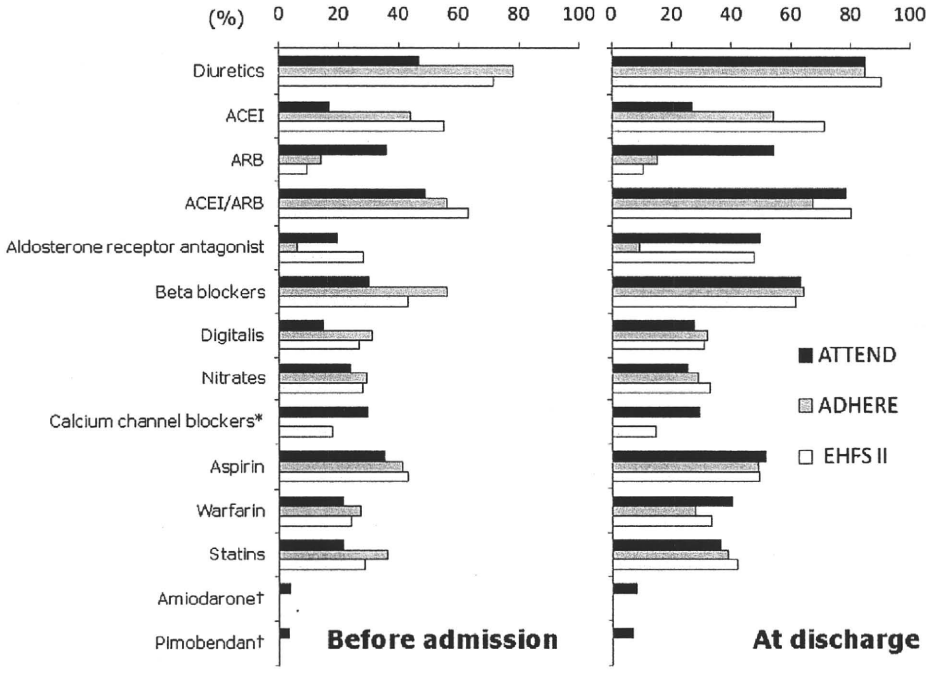

Prescribed rates of major oral medications before admission and at discharge in the present study, the acute decompensated heart failure national registry (ADHERE), and the EuroHeart failure survey II (EHFS II). Angiotensin II receptor blockers were prescribed more frequently than ACEI in the present study, which was quite different from those of Western studies.

less frequent in this study than in Western studies. However, this comparison is inappropriate because most of the Western studies included ACS. Regarding clinical status on admission, de novo AHF and orthopnea were surprisingly common in the present study, which was different from the results of Western studies. Length of hospital stay was longer than that in Western countries. This difference may be due to differences in health insurance systems or treatment and education for comorbidities during hospitalization. In-hospital mortality was relatively higher in our study, but this could be related to the greater length of hospital stay. Therefore, mortality rates for 30 days or longer should be evaluated.

Clinical profile at admission

The major symptoms and findings regarding clinical assessments are shown in Table II. Most of the patients were of New York Heart Association functional class III or IV and "warm and wet" as assessed by noninvasive hemodynamic assessments.

In-hospital management

As shown in Table III, most of the enrolled patients were treated with diuretics, mainly furosemide. Carperitide, which is a recombinant human atrial natriuretic peptide preparation that is only available in Japan, was used in 69.4% of the patients. Other vasodilators were used in about 30% of patients, and included nitroglycerin, isosorbide dinitrate, and nicorandil in 26.0%, 9.2%, and 10.6% of patients, respectively, and inotropes were administered in 20.7%. Noninvasive positive pressure ventilation (ie, continuous positive airway pressure and bilevel positive airway pressure) was performed in 21.7% and 14.4% of the patients, respectively. A Swan-Ganz catheter was inserted in 20.1%.

Oral medications before admission and at discharge: comparison with Western studies

There were differences in oral medications used before admission between the present study and the Western studies, which seems to be related to the lower rate of prior heart failure–related admission in the present study. At discharge, the prescribed rates of diuretics, angiotensin-converting enzyme inhibitors (ACEIs) or angiotensin II receptor blockers (ARBs), and β-blockers were similar to those in Western countries. Interestingly, ARBs were more frequently administered to patients with AHFS in Japan. In addition, pimobendan was prescribed in 6.6% of patients at discharge (Figure 2).

Discussion

To the best of our knowledge, the ATTEND registry is the first epidemiological study of AHFS in the Asia Pacific region. It has provided detailed data on the baseline characteristics and profile of Japanese patients with AHFS (except those with ACS) and has revealed several important differences compared with patients with AHFS in Western countries. The present study not only investigated patient characteristics but also the hemodynamic profile of patients with AHFS. Regarding the etiology of AHFS, ischemic heart disease was less common (33.2%) than that in Western registries.[14] Diuretics were used to treat most patients during hospitalization, which was similar to the management of AHFS in Western countries, although carperitide was also used in 69.4% of the patients, which was far higher than the recently reported frequency of nesiritide use in the United States (8%).[4] The use of oral medications was also somewhat different from that in Western countries because ARBs were prescribed more frequently than ACEIs. Finally, the median of length of hospital stay was longer in our registry (21 days) than in other countries.

It is important to determine the clinical characteristics and profiles of patients with AHFS in different regions because such data are necessary to evaluate whether patients are being managed appropriately in the real world according to the patient characteristics and pathophysiologic conditions in line with clinical guidelines and evidence-based medicine. If the baseline characteristics and the clinical profile are different, then the results of clinical studies performed in Western countries may not be applicable, suggesting that clinical trials on AHFS would need to be performed separately in Japan. However, data from the ATTEND registry indicate that the baseline patient characteristics, including physical findings and vital signs, were broadly similar to those shown in previous Western studies, suggesting that clinical assessments in the Western studies (eg, clinical scenarios[15] and noninvasive hemodynamic assessments[13]) might be applicable for Japanese patients and that collaboration with Western countries in clinical research or trials would be possible. In the present study, the "warm and wet" type of AHFS was observed in 73.7% of patients, which was almost the same as those in Western countries, although this has never been documented in epidemiological studies from those countries. Ischemic heart disease seems to be less common than in Western countries, but it is difficult to precisely compare the data because ischemic heart disease was defined by the presence of myocardial ischemia in the present study, whereas only the patient's history was used in other studies.[14] It is necessary to examine the baseline characteristics and the clinical profile using the same protocol to precisely compare different counties, which means that a global collaborative epidemiological study of AHFS is needed.

Carperitide was administered during hospitalization very frequently in Japan. In contrast, nesiritide was used much less frequently (8%) in Western countries,[4] possibly because meta-analyses have demonstrated no improvement of renal function[16] and poor short-term outcomes.[17] In contrast, acute low-dose carperitide infusion has been reported to improve the long-term prognosis of patients with ADHF.[18] A beneficial effect of low-dose nesiritide on renal function was recently demonstrated,[19] but low-dose nesiritide has not yet been reported to improve the long-term outcomes.

ARBs were prescribed for many patients with AHFS, which differ from that in Western countries and conflicts with clinical guidelines. One reason for this is the frequent prescription of ARBs for the management of hypertension because hypertension was highly prevalent (70.6%) in patients with AHFS and because ARBs are well tolerated, with a strong antihypertensive effect, although the guidelines used in Western countries recommend an ARB as an alternative for patients who are intolerant of an ACEI.

The hospital mortality rate was similar to that in Western countries and was strikingly similar to the 30-day mortality rate because the length of hospital stay was much longer (mean 31 days) than in Western countries (range of means 4-11 days).[14] The longer hospital stay is partly due to differences in the health insurance system and education programs for managing comorbidities during hospitalization. The results of the short-term (6-month) outcome after discharge are not yet available, but the present study is patient based rather than event based, so the readmission rate will be more precise than those obtained in other studies, and this information should be useful to improve the management of patients with AHFS.

When several epidemiological studies are being compared, there are several important issues that need to be clarified. First, what is the definition of AHFS? The modified Framingham criteria were used in the present study. We excluded change in body weight from the original criteria because the physician cannot estimate it at admission. The definition of AHFS should be based on data available at the time of admission. In addition, brain natriuretic peptide levels at admission were not included for the diagnosis of AHFS because a cutoff value has not yet been defined for Japanese patients, although the data were collected in the present study. In some studies, the definition for AHFS was not clarified. In particular, it should be clarified whether patients with ACS are included in the study. In the ATTEND study, patients with ACS are excluded because the management of ACS is quite different from that for other patients with AHFS. Thus, the criteria for the diagnosis of AHFS should be discussed and defined more precisely. Second, the setting to which the enrolled patients are admitted (ie, cardiac care unit, emergency department, or general ward)

should be recorded because this influences the characteristics of patients with AHFS and the outcomes. For example, the short-term prognosis was worse in the EFICA study[20] than in other studies because all patients were admitted to an intensive care unit, which means that more critical patients with AHFS were enrolled. The ATTEND registry includes several intensive care units and cardiac care units. Therefore, the characteristics of the participating hospitals will be considered in the final analysis. Third, how should patients with AHFS be evaluated clinically? The ATTEND registry not only records physical findings but also noninvasive hemodynamic assessments. Based on European guidelines, noninvasive hemodynamic assessments are commonly used in clinical settings to assess the characteristics of patients with AHFS; however, its validity for AHFS has not yet been confirmed in scientific studies. Therefore, the present study will provide useful information regarding its merits and limitations.

In conclusion, data from the ATTEND registry have demonstrated the clinical characteristics of patients with AHFS in Japan. This ongoing study will continue to provide valuable information regarding the pathophysiologic, therapeutic, and prognostic issues related to AHFS, such as new clinical scenarios.

Acknowledgements

We thank Dr Mihai Gheorghiade for his critical review of our article. We also thank all investigators for their contributions.

References

1. Hunt SA, Abraham WT, Chin MH, et al. Focused Update Incorporated Into the ACC/AHA 2005 Guidelines for the Diagnosis and Management of Heart Failure in Adults. A Report of the American College of Cardiology Foundation/American Heart Association Task Force on Practice Guidelines. J Am Coll Cardiol 2009;53:e1-e90.
2. Lloyd-Jones D, Adams R, Carnethon M, et al. Heart Disease and Stroke Statistics – 2009 Update: A Report from the American Heart Association Statistics Committee and Stroke Statistics Subcommittee. Circulation 2009;119:480-6.
3. McLean AS. Epidemiology and management of acute decompensated heart failure in the Asia-Pacific region. In: Mebazaa A, Gheorghiade M, Zannad FM, Parrillo JE, editors. Acute Heart Failure. Springer-Verlag London Limited; 2008. p. 20-9.
4. The ADHERE (Acute Decompensated Heart Failure National Registry) Registry. Background and Q1 2006 Final Cumulative Benchmark Report. Available at: http://www.sciosinc.com/sciosinc/adhere.html.
5. Fonarow GC, Heywood JT, Heidenreich PA, et al, for the ADHERE Scientific Advisory Committee and Investigators. Temporal trends in clinical characteristics, treatments and outcomes for heart failure hospitalizations, 2002 to 2004: findings from Acute Decompensated Heart Failure National Registry (ADHERE). Am Heart J 2007;153: 1021-8.
6. Adams Jr KF, Fonarow GC, Emerman CL, et al, for the ADHERE Scientific Advisory Committee and Investigators. Characteristics and outcomes of patients hospitalized for heart failure in the United States: rationale, design, and preliminary observations from the first 100,000 cases in the Acute Decompensated Heart Failure National Registry (ADHERE). Am Heart J 2005;149:209-16.
7. Gheorghiade M, Filippatos G, De Luca L, et al. Congestion in acute heart failure syndromes: an essential target of evaluation and treatment. Am J Med 2006;119(12A):S3-S10.
8. Gheorghiade M, Abraham WT, Albert NM, et al, for the OPTIMIZE-HF investigators and coordinators. Systolic blood pressure at admission, clinical characteristics, and outcomes in patients hospitalized with acute heart failure. JAMA 2006;296:2217-26.
9. Nieminen MS, Brutsaert D, Dickstein K, et al, on behalf of the EuroHeart Survey investigators. Heart Failure Survey II (EHFS II): a survey on hospitalized acute heart failure patients: description of population. Eur Heart J 2006;27:2725-36.
10. Uniform Requirements for Manuscripts Submitted to Biomedical Journals: Writing and Editing for Biomedical Publication. Publication Ethics: Sponsorship, Authorship, and Accountability International Committee of Medical Journal Editors. Available at: http://www.icmje.org/index.html.
11. McKee PA, Castelli WP, McNamara PM, et al. The natural history of congestive heart failure: the Framingham study. N Engl J Med 1971; 285:1441-6.
12. Radford MJ, Arnold JM, Bennett SJ, et al. ACC/AHA heart failure clinical data standards. ACC/AHA Key Data Elements and Definitions for Measuring the Clinical Management and Outcomes of Patients With Chronic Heart Failure. A Report of the American College of Cardiology/American Heart Association Task Force on Clinical Data Standards (Writing Committee to Develop Heart Failure Clinical Data Standards). J Am Coll Cardiol 2005;46:1179-207.
13. Nohria A, Mielniczuk LM, Stevenson LW. Evaluation and monitoring of patients with acute heart failure syndromes. Am J Cardiol 2005;96 (Suppl):32G-40G.
14. Alla F, Zannad F, Filippatos G. Epidemiology of acute heart failure syndromes. Heart Fail Rev 2007;12:91-5.
15. Mebazaa A, Gheorghiade M, Piña IL, et al. Practical recommendations for prehospital and early in-hospital management of patients presenting with acute heart failure syndromes. Crit Care Med 2008; 36(Suppl):S129-39.
16. Sackner-Bernstein JD, Skopicki HA, Aaronson KD. Risk of worsening renal function with nesiritide in patients with acutely decompensated heart failure. Circulation 2005;111:1487-91.
17. Sackner-Bernstein JD, Kowalski M, Fox M, et al. Short-term risk of death after treatment with nesiritide for decompensated heart failure: a pooled analysis of randomized controlled trials. JAMA 2005;293: 1900-5.
18. Hata N, Seino Y, Tsutamoto T, et al. Effects of carperitide on the long-term prognosis of patients with acute decompensated chronic heart failure: the PROTECT multicenter randomized controlled study. Circ J 2008;72:1787-93.
19. Riter HG, Redfield MM, Burnett JC, et al. Nonhypotensive low-dose nesiritide has differential renal effects compared with standard-dose nesiritide in patients with acute decompensated heart failure and renal dysfunction. JACC 2006;47:2334-5.
20. Zannad F, Mebazaa A, Cohen-Solal A, et al, for the EFICA Investigators. Clinical profile, contemporary management and one-year mortality in patients with severe acute heart failure syndromes: the EFICA study. Eur J Heart Fail 2006;8:697-705.

Appendix

ATTEND Scientific Advisory Committee:

Executive Committee: Takano T (chair), Kasanuki H, Tanaka K, Mizuno K

Data and Safety Monitoring Board: Meguro T, Sato T

End point Committee: Kawana M, Nejima J

Statistical Data Center: Katsunori Shimada (STATZ Institute Inc)

Steering Committee: Kajimoto K, Asai K, Mizuno M, Yumino D, Minami Y, Murai K, Munakata R, Sato N

Study Investigators (47 hospitals)

Asahikawa Medical College Hospital: Takeuchi T, Okada M, Hasebe N

Edogawa Hospital: Keida T, Fujita M, Nakamura K, Chinenn T, Meguro K, Kikuchi T, Nishikido T

Fukui Cardiovascular Center: Moriuchi I

Fukushima Medical University Hospital: Yoshihisa S, Sato T, Takeishi K

Gunma Prefectural Cardiovascular Center: Yamashita E, Toyama T

Hyogo College of Medicine Hospital: Kawabata M, Fujii K

Hyogo Prefectural Amagasaki Hospital: Sato Y

Kitamurayama Hospital: Yoshida A

Komaki City Hospital: Kondo T, Kawaguchi K, Shimazu S

Komatsu Municipal Hospital: Kaneda T, Ueda Y

Kurashiki Central Hospital: Hirono A, Mistudo K, Kadota K, Makita N, Watanabe N

Kure Medical Center: Yamashita Y

Kyushu University Hospital: Todaka K

Mitsubishi Kyoto Hospital: Mizuguchi T

Nagasaki University Hospital: Koide Y, Maemura K

Nigigaoka Hospital: Kawahara F

Niigata Prefectural Central Hospital: Masani F

Nippon Medical School Hospital: Sato N, Asai K, Munakata R, Murai K

Nippon Medical School, Chiba-Hokusoh Hospital: Hata N

Oji General Hospital: Ishii K, Ooiwa H, Matsumoto T, Yoshida D, Kato N

Osaka City General Hospital: Komatsu R, Abe Y, Ito A

Osaka Police Hospital: Kashiwase K, Ueda Y

Osaka University Hospital: Sakata Y, Komuro I

Saiseikai Kumamoto Hosipital: Nakao K, Sawamura K, Nuki T, Shoji M, Takahashi N

Saiseikai Kurihashi Hospital: Mizuno M

Seirei Hamamatsu Hospital: Kamishima K, Oka T

Sendai Cardiovascular Center: Fujimori K, Kobayashi H, Fujii S, Yagi K, Sasaki J

Sensoji Hospital: Kajimoto K

Shiga University of Medical Science: Tsutamoto T

Shizuoka Medical Center: Kawanaka H, Tanabe J

Shonan Dai-ichi Hospital: Nagashima M, Shimamura K

Showa University Hospital: Sakai T

Showa University, Fujigaoka Hospital: Suzuki H, Shimizu N

Suwa Central Hospital: Imai T

Tokai University Hospital: Yoshioka K

Tokushima Prefectural Central Hospital: Fujinaga H, Yamamoto T, Harada K, Saito A, Kageyama N, Okumura U

Tokyo Medical University Hospital: Takata Y

Tokyo Medical University, Hachioji Medical Center: Teraoka K

Tokyo University Hospital: Imai Y

Tokyo Women's Medical University Hospital: Minami Y, Yoshida K, Yumino D, Kawada E, Ozaki Y, Haruki S, Kogure T

Tokyo Women's Medical University, Aoyama Hospital: Kajimoto K

Tokyo Women's Medical University, Medical Center East: Okajima K, Nunoda S

Tottori University Hospital: Kato M

Toyota Memorial Hospital: Ishii R, Yokota S

Yamaguchi University Hospital: Okuda S, Kobayashi S

Yatsu Hoken Hospital: Sudo S

Yokohama City Medical Center: Ebina T, Kimura K

Dynamic Expression of Tenascin-C After Myocardial Ischemia and Reperfusion: Assessment by ^{125}I-Anti–Tenascin-C Antibody Imaging

Junichi Taki[1], Anri Inaki[1], Hiroshi Wakabayashi[1], Kyoko Imanaka-Yoshida[2], Kazuma Ogawa[3], Michiaki Hiroe[4], Kazuhiro Shiba[5], Toshimichi Yoshida[2], and Seigo Kinuya[1,6]

[1]Department of Nuclear Medicine, Kanazawa University Hospital, Kanazawa, Japan; [2]Department of Pathology, Mie University School of Medicine, Mie, Japan; [3]Graduate School of Natural Science and Technology, Kanazawa University, Kanazawa, Japan; [4]Department of Nephrology and Cardiology, International Medical Center of Japan, Tokyo, Japan; [5]Division of Tracer Kinetics, Advanced Science Research Center, Kanazawa University, Kanazawa, Japan; and [6]Department of Biotracer Medicine, Kanazawa University Graduate School of Medical Sciences, Kanazawa, Japan

Tenascin-C, an extracellular matrix glycoprotein, appears only in the early stages of embryonic development. It is not normally expressed in the adult heart but does reappear transiently in distinct areas in association with active tissue remodeling. The aim of this study was to explore serial changes in the expression of tenascin-C after myocardial ischemia and reperfusion, using ^{125}I-labeled anti–tenascin-C antibody (^{125}I-TNC-Ab) in a rat model of acute ischemia and reperfusion. **Methods:** The left coronary artery was occluded for 20 or 30 min, followed by reperfusion for 1, 3, or 7 d in rats with 20 min of ischemia and for 1, 3, 7, 14, or 28 d in rats with 30 min of ischemia. At the time of the study, ^{125}I-TNC-Ab (1.0–2.5 MBq) was injected. Three to 5 h later, to verify the area at risk, ^{99m}Tc-methoxyisobutylisonitrile (100–200 MBq) was injected intravenously just after the left coronary artery reocclusion and the rats were sacrificed 1 min later. Dual-tracer autoradiography was performed to assess ^{125}I-TNC-Ab uptake and the area at risk. **Results:** In rats with 20 min of ischemia, ^{125}I-TNC-Ab uptake peaked at 3 d after reperfusion, followed by faint uptake after 7 d (uptake ratios at 1, 3, and 7 d after reperfusion were 1.81 ± 0.53, 2.46 ± 0.79, and 1.23 ± 0.17, respectively [$P < 0.05$ vs. 3 d]). In rats with 30 min of ischemia, uptake was high at 1 and 3 d after reperfusion (2.99 ± 0.90 and 2.71 ± 0.80, respectively), decreased at 7 and 14 d (1.94 ± 0.23 and 2.06 ± 0.37, respectively), and was weak at 28 d (1.47 ± 0.27, $P < 0.005$ vs. 1 d, $P < 0.05$ vs. 3 d). **Conclusion:** These data indicate that ^{125}I-TNC-Ab imaging may be a way to monitor myocardial injury and its repair process after ischemia and reperfusion by visualizing tenascin-C expression.

Key Words: tenascin-C; ^{125}I-anti–tenascin-C-antibody; myocardial ischemia; reperfusion; autoradiography

J Nucl Med 2010; 51:1116–1122
DOI: 10.2967/jnumed.109.071340

Received Oct. 5, 2009; revision accepted Mar. 17, 2010.
For correspondence or reprints contact: Junichi Taki, Department of Nuclear Medicine, Kanazawa University Hospital, 13-1 Takara-machi, Kanazawa, 920-8641, Japan.
E-mail: taki@med.kanazawa-u.ac.jp

Cardiac repair after myocardial infarction is regulated thorough activation and repression of the acute inflammatory process, followed by timely infiltration of the infarcted myocardium with myofibroblasts. These secrete large amounts of extracellular matrix proteins, leading to formation of collagen-based scar tissue in the infarct. Inflammatory and fibrotic processes are critically involved in the pathogenesis of ventricular remodeling, which is a significant predictor of left ventricular dysfunction and an adverse prognosis (*1*). Extracellular matrix and cardiac cells are essential for maintaining the integrity of cardiac tissue and play an important role not only in structural and mechanical support but also in modulation of cell function.

It has been reported that tenascin-C, an extracellular matrix glycoprotein, could provide important biologic signaling that influences cell motility, proliferation, differentiation, survival, or apoptosis via cellular–extracellular matrix interaction during remodeling of various tissues (*2,3*). Tenascin-C appears in the heart only in the early stages of embryonic development and is not normally expressed in adults. However, it reappears transiently in association with myocardial injury such as myocardial infarction (*4–6*), hibernating myocardium (*7*), myocarditis (*6,8,9*), and dilated cardiomyopathy (*10,11*). Its site-specific expression suggests that tenascin-C plays important roles during tissue remodeling but also that it can serve as an indicator of myocardial disease activity.

Recently, we and other groups have reported increased serum tenascin-C in heart failure patients, reflecting the severity and progression of ventricular remodeling (*12–15*). Of particular interest is that patients with acute myocardial infarction with high serum levels of tenascin-C within 1 wk of infarction have a greater incidence of ventricular remodeling 6 mo later and a worse long-term prognosis

(*16*), indicating that tenascin-C can be a possible predictor of ventricular remodeling and poor prognosis after myocardial infarction. These considerations make it important to assess the expression of tenascin-C in the acute phase of myocardial infarction.

In previous animal studies on acute myocardial infarction induced by permanent ligation of a coronary artery, it was reported that tenascin-C appears transiently during the acute stage, plays several significant roles in myocardial tissue remodeling, and may be a potential candidate for molecular imaging (*9,17*). For clinical application of the imaging, it is essential to analyze the molecular dynamics in the model of myocardial ischemia and reperfusion that is the general scenario in the era of percutaneous coronary intervention in acute coronary syndrome.

The aim of this study was to explore spatial and temporal changes in the expression of tenascin-C after myocardial ischemia and reperfusion using ^{125}I-labeled anti–tenascin-C antibody (^{125}I-TNC-Ab) in a rat model of acute ischemia and reperfusion.

MATERIALS AND METHODS

Animal Model of Acute Ischemia and Reperfusion

All experimental procedures involving animals were conducted in accordance with the institutional guidelines set by the Institute for Experimental Animals, Kanazawa University Advanced Science Research Center. Ten- to 14-wk-old male Wistar rats (n = 51) were anesthetized with an intraperitoneal administration of 40 mg of pentobarbital per kilogram of body weight and ventilated mechanically with room air. After left thoracotomy and exposure of the heart, a 7–0 polypropylene suture on a small curved needle was passed through the myocardium beneath the proximal portion of the left coronary artery (LCA), and both ends of the suture were passed through a small vinyl tube to make a snare. The suture material was pulled tightly against the vinyl tube to occlude the LCA. Myocardial ischemia was confirmed by regional cyanosis of the myocardial surface and ST-segment elevation on the electrocardiograph. Two series of experiments were performed. The first evaluated a 20-min interval of LCA occlusion and reperfusion, and the second evaluated a 30-min interval of LCA occlusion and reperfusion, to determine the distribution of tenascin-C expression. Reperfusion was obtained by release of the snare and was confirmed by a myocardial blush over the area at risk. The snare was left loose on the surface of the heart until repeated thoracotomy for reocclusion of the LCA just before sacrifice to identify the area at risk (*18*). Groups of animals with 20 min of occlusion were studied at 1 d (n = 6), 3 d (n = 5), and 7 d (n = 5) after reperfusion, and groups of animals with 30 min of occlusion were studied at 1 d (n = 6), 3 d (n = 6), 7 d (n = 5), 14 d (n = 6), and 28 d (n = 6) after reperfusion. At the time of the study, ^{125}I-TNC-Ab (1.0–2.5 MBq) was administered via a tail vein. In 6 rats with 30 min of ischemia and 3 d of reperfusion, 1.5–2.0 MBq of ^{125}I-labeled nonspecific antibody were injected. Three to 5 h afterward, 100–200 MBq of ^{99m}Tc-methoxyisobutylisonitrile (MIBI) were injected via a tail vein just after reocclusion of the proximal portion of the LCA for delineation of the area at risk. One minute later, the rat was euthanized and the heart was removed for analysis. The excised heart was rinsed in saline, frozen in isopentane, cooled in dry ice, and embedded in methyl cellulose. Serial short-axis heart sections 20 μm thick were obtained on a cryostat to create a series of rings for autoradiography.

Biodistribution Study

Biodistribution was studied in rats with 30 min of ischemia and 3 d of reperfusion with injection of 1.5–2.0 MBq of ^{125}I-TNC-Ab. Groups of rats were euthanized at 1 h (n = 4), 5 h (n = 5), and 24 h (n = 5) after tracer injection. Hearts (nonischemic area and infarcted area), other organs (lung, liver, spleen, kidney, and muscle), and blood were weighed and then counted for radioactivity to calculate the percentage injected dose per gram of tissue.

Radiolabeling of Anti-Tenascin C Antibody

Anti–tenascin-C mouse IgG Fab′, a mouse monoclonal antibody against tenascin-C, clone 4F10TT, was raised by immunization of a tenascin-C–null mouse with purified human tenascin-C as described previously (*6*).

Anti–tenascin-C antibody was radiolabeled with ^{125}I by the chloramine-T method (*19*). Briefly, ^{125}I-sodium iodide solution (37 MBq/10 μL; Perkin Elmer) was added to 60 μL of antibody in phosphate-buffered saline (0.32 mg/mL). After mixing, 4 μL of chloramine-T aqueous solution (1 mg/mL) were added. After 15 min at room temperature, the reaction was quenched with 20 μL of $Na_2H_2SO_5$. The crude product was purified with a PD-10 column (GE Healthcare U.K., Ltd.) with saline as the eluate. The radiochemical purity of ^{125}I-TNC-Ab was determined by thin-layer chromatography, which was performed with silica plates (catalog no. 5553; Merck) and with saline as the developing solvent. Radiochemical purity was defined as the percentage of protein-bound activity, which was assessed by dividing counts at the thin-layer chromatography origin by total thin-layer chromatography counts.

As a nonspecific control antibody, mouse F(ab′)$_2$ IgG1 (Beckman Coulter, Inc.) was reduced to Fab′ with 50 mM 2-mercaptoethylamine in phosphate-buffered saline containing 10 mM ethylenediaminetetraacetic acid at 37°C for 1 h. Radiolabeling of the control antibody (Fab′) with ^{125}I was performed as described above.

Dual-Tracer Autoradiography

Dual-tracer autoradiography of the left ventricular short-axis slices was performed for the assessment of ^{125}I-TNC-Ab uptake and ischemic area (^{99m}Tc-MIBI image). The first autoradiographic exposure on an imaging plate (BAS-MS; Fuji Film) was performed for 15–20 min to visualize the area at risk as expressed by ^{99m}Tc-MIBI distribution at 1–2 h after sacrifice. Three days later (12 half-lives of ^{99m}Tc), the second exposure was made for 7 d to image the distribution of ^{125}I-TNC-Ab.

Data Analysis

^{125}I-TNC-Ab accumulation was evaluated in 3 myocardial slices at the mid–ventricular level spaced 1 mm apart from one another. The distribution of the tracers was determined by analysis of the digitized autoradiographs. The photostimulated luminescence in each pixel (100 × 100 μm) was determined using a bioimaging analyzer (BAS-5000; Fuji Film). For quantitative analysis, the uptake values of each region of interest (ROI) were expressed as the background-corrected photostimulated luminescence per unit area (1 mm^2). A background ROI was set adjacent to the left ventricle. Ischemic and normally perfused areas were

defined from the ^{99m}Tc-MIBI image, and these ROIs were applied to the ^{125}I-TNC-Ab images to evaluate the uptake of ^{125}I-TNC-Ab. An area of significant ^{125}I-TNC-Ab uptake was also defined manually as an ROI. The ^{125}I-TNC-Ab uptake ratio was calculated by dividing the uptake value in an ischemic area by that of a normally perfused area. The ratio of a ^{125}I-TNC-Ab uptake ROI to an ischemic ROI was defined as the percentage of the ^{125}I-TNC-Ab uptake area (*18*). All parameters in each rat were expressed as the average value obtained from the analysis of 3 representative slices.

Immunohistochemical Staining

Short-axis frozen sections adjacent to the slices for autoradiography were mounted on slides. These short-axis heart sections were washed with phosphate-buffered saline and stained with mouse anti–tenascin-C antibody 4F10TT, the same antibody used for autoradiography, using direct immunoperoxidase technique. For paraffin sections, the heart was fixed in 4% paraformaldehyde, embedded in paraffin, and immunostained as previously described (*5*). Briefly, after treatment with pepsin for 10 min for antigen retrieval, sections were incubated with anti–tenascin-C antibody 4F10TT and subsequently with peroxidase-conjugated antimouse IgG Fab′ (Medical and Biological Lab Co., Ltd.). After washing, diaminobenzidine/H_2O_2 solution was used to demonstrate antibody binding. The site and distribution of the expression of tenascin-C were examined with the aid of the hematoxylin- and eosin-stained slice adjacent to the immunohistochemically stained slice.

Statistical Analysis

All results were expressed as mean ± SD. Statistical analyses were performed using a Macintosh computer (Apple) with JMP software (version 5.0.1J; SAS Institute, Inc.). Groups were compared using the Tukey–Kramer method. A value of P less than 0.05 was considered statistically significant.

RESULTS

Radiolabeling

^{125}I-TNC-Ab was prepared with high radiochemical yield (89%). After purification by PD-10, ^{125}I-TNC-Ab showed a radiochemical purity of over 99%.

Area with ^{125}I-TNC-Ab Uptake Versus Area at Risk

The percentages of ^{125}I-TNC-Ab uptake areas against areas at risk in rats with 20 min of ischemia at 1, 3, and 7 d after reperfusion were similar (59.5% ± 10.4%, 52.9% ± 4.0%, and 62.3% ± 3.1%, respectively; not statistically significant) (Fig. 1).

In rats after 30 min of reperfusion, the percentages of ^{125}I-TNC-Ab uptake areas at 1, 3, 7, 14, and 28 d after reperfusion tended to decrease with longer reperfusion periods (70.2% ± 8.2%, 63.7% ± 4.3%, 63.5% ± 3.7%, 61.0% ± 14.3%, and 52.3% ± 13.0%, respectively), but statistical significance was observed only when 1 d was compared with 28 d ($P < 0.05$) (Fig. 1).

When ^{125}I-TNC-Ab uptake areas against areas at risk were compared between rats with 20 and 30 min of ischemia, the uptake areas of rats with 30 min of ischemia were larger than those of rats with 20 min of ischemia only at 3 d after reperfusion ($P < 0.05$).

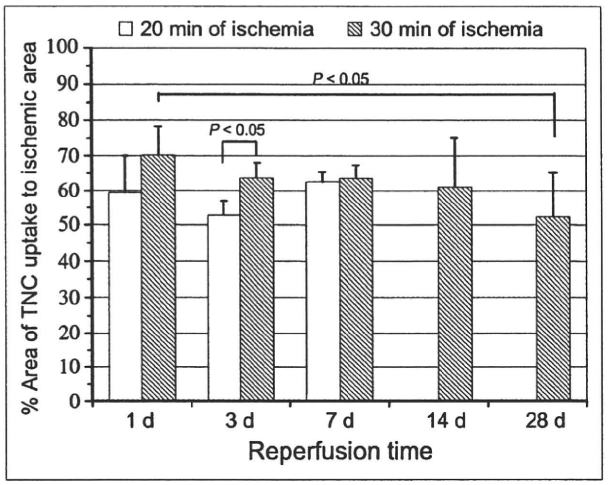

FIGURE 1. Time course of ^{125}I-TNC-Ab uptake area against area at risk (% area). In rats with 20 min of ischemia, area of tenascin-C uptake was similar among 1, 3, and 7 d after reperfusion. In rats with 30 min of ischemia, area was also similar among 1, 3, 7, 14 and 28 d except for significant difference only when day 1 was compared with day 28.

^{125}I-TNC-Ab Uptake

In visual analysis, significant ^{125}I-TNC-Ab uptake was observed predominantly in the midmyocardial to endomyocardial layers in the area at risk in rats with 20 min of ischemia at 1 d after reperfusion, and the intensity increased at 3 d followed by faint uptake at 7 d. In rats with 30 min of ischemia, strong ^{125}I-TNC-Ab uptake was also observed in the midmyocardial to endomyocardial layers in the area at risk at 1 and 3 d after reperfusion, followed by moderate uptake at 7 and 14 d and weak uptake at 28 d (Fig. 2).

In the quantitative analysis, the ^{125}I-TNC-Ab uptake ratio of the rats with 20 min of ischemia was 1.81 ± 0.53 at 1 d after reperfusion and increased at 3 d (2.46 ± 0.79), followed by a significant reduction at 7 d (1.23 ± 0.17, $P < 0.05$ vs. 3 d). The uptake ratio of the rats with 30 min of ischemia at 1 and 3 d after reperfusion was equally high (2.99 ± 0.90 and 2.71 ± 0.80, respectively); the uptake decreased at 7 and 14 d (1.94 ± 0.23 and 2.06 ± 0.37, respectively) and then was weak at 28 d (1.47 ± 0.27, $P < 0.005$ vs. 1 d, $P < 0.05$ vs. 3 d). When rats with 20 and 30 min of ischemia were compared, ^{125}I-TNC-Ab uptake in rats with 30 min of ischemia was higher at 1 d ($P < 0.05$) and 7 d ($P < 0.001$) after reperfusion but was similar at 3 d (Fig. 3).

^{125}I-labeled nonspecific antibody accumulated only slightly in the ischemic area (uptake ratio, 1.36 ± 0.27) in rats with 30 min of ischemia at 3 d after reperfusion. This uptake was significantly lower ($P < 0.005$) than that of ^{125}I-TNC-Ab (2.71 ± 0.80).

Biodistribution of ^{125}I-TNC-Ab

As shown in Table 1, uptake of ^{125}I-TNC-Ab in the infarcted area was 0.53 ± 0.089, 0.62 ± 0.13, and 0.27 ±

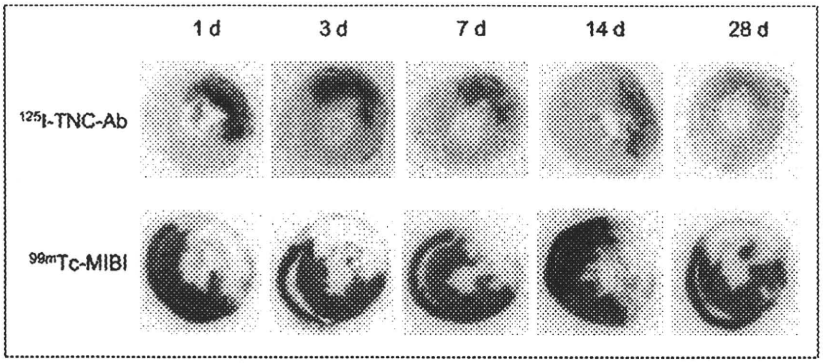

FIGURE 2. Autoradiography of ^{125}I-TNC-Ab and ^{99m}Tc-MIBI in rats with 30 min of ischemia. Intense ^{125}I-TNC-Ab uptake was observed predominantly in midmyocardial to endomyocardial layers at 1 and 3 d after reperfusion. Reduced but significant ^{125}I-TNC-Ab uptake persisted at 7 and 14 d, followed by obvious reduction of uptake at 28 d.

0.11 percentage injected dose per gram of tissue at 1, 5, and 24 h after tracer injection, respectively. Because of the rapid blood clearance of ^{125}I-TNC-Ab and good retention in infarcted areas, a decent infarcted area–to–blood ratio was obtained at 5 and 24 h after injection (1.85 ± 0.14 and 4.8 ± 1.0, respectively), and the infarcted area–to–lung ratio at 5 and 24 h after tracer injection was 1.97 ± 0.19 and 4.9 ± 1.2, respectively, suggesting feasibility for in vivo imaging. However, liver uptake that was relatively high but less than double the infarcted area was observed until 24 h.

Histopathologic Findings

The accumulation of ^{125}I-TNC-Ab seen on autoradiography corresponded closely to the area with positive immunohistopathologic staining by ^{125}I-TNC-Ab. Representative cases are shown in Figure 4A.

One to 3 d after 30 min of ischemia and reperfusion, coagulation necrosis of cardiomyocytes and severe inflammatory cell infiltration were apparent in the infarcted area. Tenascin-C deposition and inflammation were observed throughout the infarcted area. Especially strong staining was noted at the border zone. No tenascin-C expression was detected in the intact area (Fig. 4B). Necrotic tissue was gradually replaced by granulation tissue, with attenuation of inflammation. Tenascin-C deposition gradually decreased and had almost disappeared on day 28, when collagen fiber–rich scar tissue had formed in the injured lesion.

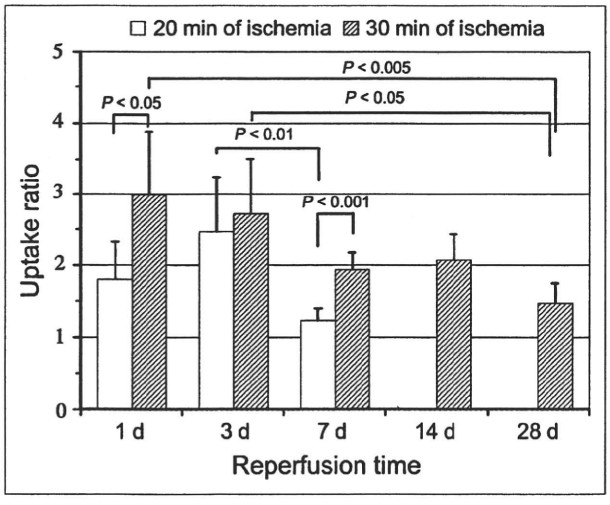

FIGURE 3. Time course of ^{125}I-TNC-Ab uptake ratio in rats with 20 and 30 min of ischemia. ^{125}I-TNC-Ab uptake ratio was calculated by dividing ^{125}I-TNC-Ab count density in area at risk by that of nonischemic area. In rats with 20 min of ischemia, ^{125}I-TNC-Ab uptake was significant at 1 d after reperfusion and peaked at 3 d, followed by marked reduction at 7 d. In rats with 30 min of ischemia, ^{125}I-TNC-Ab uptake ratio was highest at 1 and 3 d, followed by reduction at 7 and 14 d. Further reduction of uptake ratio was observed at 28 d.

DISCUSSION

The present study demonstrated the feasibility of imaging targeted at tenascin-C expression and documented for the first time, to our knowledge, spatiotemporal profiling of tenascin-C expression after myocardial ischemia and reperfusion. In myocardium with 20 min of ischemia and reperfusion, significant tenascin-C expression was observed inhomogeneously but predominantly in the midmyocardial to endomyocardial layers within the area at risk at 1 d after reperfusion, and the expression peaked at 3 d, followed by a marked reduction of tenascin-C expression at 7 d. However, when the ischemia was prolonged to 30 min, the time course of the tenascin-C expression differed considerably; it peaked at 1 and 3 d after reperfusion, and a reduced but still significant expression persisted over 7–14 d, followed by an obvious decline in tenascin-C expression at 28 d. We surmise that in the model of ischemia and reperfusion, the duration of coronary artery occlusion or the severity of ischemia is the most potent factor determining the degree and time course of tenascin-C expression. Histopathologic examination also demonstrated similar results obtained from autoradiography. More prolonged tenascin-C immunostaining was observed in the model of 30 min of ischemia and reperfusion than in the model of 20 min of ischemia.

A previous immunohistopathologic study on rats with permanent coronary ligation demonstrated interstitial positive tenascin-C immunoreactivity in the border zone

TABLE 1. Biodistribution of ^{125}I-TNC-Ab

Tissue	Time after intravenous administration		
	1 h	5 h	24 h
Blood	0.59 ± 0.069	0.33 ± 0.063	0.057 ± 0.020
Heart (norm)	0.22 ± 0.018	0.16 ± 0.026	0.059 ± 0.035
Heart (inf)	0.53 ± 0.089	0.62 ± 0.13	0.27 ± 0.11
Liver	0.97 ± 0.43	0.99 ± 0.28	0.34 ± 0.099
Lung	0.48 ± 0.39	0.32 ± 0.068	0.054 ± 0.012
Spleen	0.67 ± 0.29	0.41 ± 0.039	0.089 ± 0.017
Muscle	0.063 ± 0.052	0.077 ± 0.023	0.020 ± 0.0064
Kidney	1.23 ± 0.71	0.87 ± 0.084	0.24 ± 0.11
Heart (inf)/blood	0.91 ± 0.087	1.85 ± 0.14	4.8 ± 1.0
Heart (inf)/lung	1.20 ± 0.71	1.97 ± 0.19	4.9 ± 1.2
Heart (inf)/liver	0.69 ± 0.45	0.66 ± 0.16	0.82 ± 0.25

Inf = infarcted area; norm = normal area.
Data are mean (±SD) percentage injected dose per gram of tissue.

between infarcted and intact areas at 1 d after ligation. Approximately 3 d after ligation, necrotic myocardium began to be replaced by granulation tissue, and tenascin-C immunoreactivity was observed at the marginal zone and at developing fronts of granulation tissue around necrotic cardiomyocytes (*5*). However, in the present study with ischemia and reperfusion, ^{125}I-TNC-Ab accumulation and tenascin-C immunostaining were scattered throughout but restricted within the ischemic area at 1 d after reperfusion. Three days after reperfusion granulation, tissues were formed intricately in the midmyocardial to endomyocardial layers, with a vague border, and tenascin-C immunoreactivity was observed rather widely around granulation tissue. This finding can be explained by the presence of scattered surviving foci of myocardial tissue in the infarcted area because of tissue salvage by reperfusion.

After myocardial infarction, tenascin-C is markedly but transiently upregulated during the early phase of tissue repair, is predominantly produced by interstitial fibroblasts, and is localized in the border zone between infarcted and viable myocardium (*4,5*). Tenascin-C may have a dual role in cardiac tissue repair and healing. Tenascin-C may loosen cardiomyocytes from the matrix, causing slippage of cardiomyocytes, and may facilitate inflammatory cell infiltration. Tenascin-C upregulates the transcription and activity of matrix metalloproteinases (*20,21*), thereby promoting degradation of the extracellular matrix and slippage of myocytes within the ventricular wall, resulting in an increased risk of ventricular thinning and dilatation. On the other hand, tenascin-C may increase matrix production, resulting in reinforcement of the cardiac matrix (*5,6,22*). A timely and proper degree of tenascin-C expression might

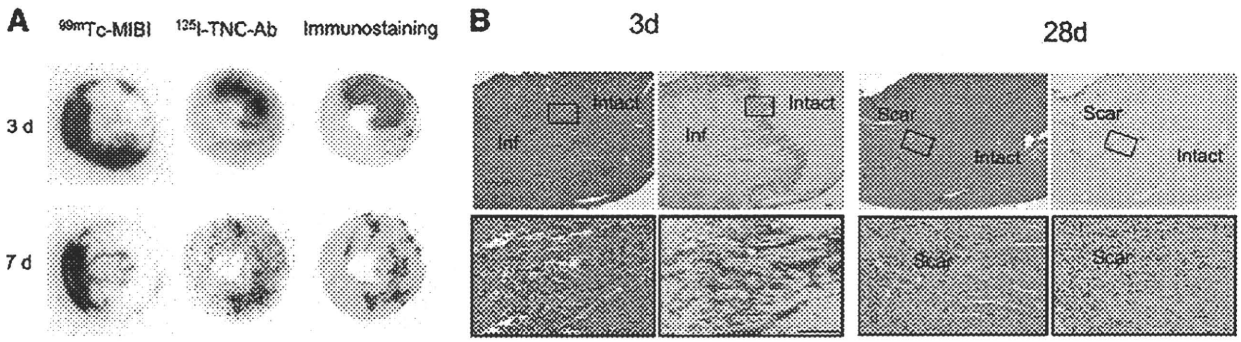

FIGURE 4. (A) Comparison of autoradiography of ^{125}I-TNC-Ab and immunostaining. Distribution of ^{125}I-TNC-Ab and immunoreactivity were well colocalized in both models at 3 and 7 d after 30 min of ischemia and reperfusion. (B) Tenascin-C expression in myocardium at 3 and 28 d after 30 min of ischemia and reperfusion (hematoxylin–eosin staining on left and immunostaining for tenascin-C on right). Images at bottom are enlargements of boxed areas in images at top. Three days after reperfusion, coagulation necrosis of cardiomyocytes and severe inflammatory cell infiltration were seen in infarcted area (left images), and tenascin-C deposition was seen in infarcted area but not in intact area (right images), with especially strong staining noted at border zone. Twenty-eight days after reperfusion, collagen-rich scar tissue had formed in injured area (left images), and tenascin-C staining had largely disappeared (right images). Bar = 100 μm; inf = infarcted area; intact = intact area; scar = scar tissue.

benefit myocardial tissue repair, whereas prolonged overexpression of tenascin-C might interfere with sound tissue repair and cause inappropriate reconstruction of the infarcted ventricle, resulting in so-called ventricular remodeling. In patients with acute myocardial infarction, the peak serum tenascin-C level at 5 d after infarction is an important independent predictor of prognosis. A higher tenascin-C level is associated with a greater risk of left ventricular remodeling at 6 mo after infarction, indicating that overexpression of tenascin-C may aggravate ventricular remodeling (*16*). Furthermore, Frangogiannis et al. revealed that, in patients with severe chronic ischemic heart disease, dysfunctional myocardial segments expressing more tenascin-C showed significantly better functional recovery after bypass surgery than did segments without tenascin-C expression. Expression of tenascin-C in the dysfunctional segment may suggest that active continuous fibrosis is in progress in that area and may be beneficial for surgical interventional revascularization therapy to prevent ventricular remodeling (*7*).

The application of targeted radionuclide imaging of regional tenascin-C expression as proposed in the present study holds the potential to quantify the extent, amount, and localization of tenascin-C expression in vivo and to relate pathophysiologic events to tissue repair and remodeling after severe myocardial ischemia. Furthermore, the proposed imaging approach would provide the opportunity to monitor novel therapeutic interventions directed toward the reduction of extracellular matrix remodeling after myocardial infarction. Although the current study demonstrated changes in spatiotemporal ^{125}I-TNC-Ab accumulation after myocardial ischemia and reperfusion, further study should investigate the relationship between the degree or temporal prolongation of ^{125}I-TNC-Ab uptake and ventricular dilatation or remodeling after myocardial infarction. In addition, assessments of whether interventional therapy to protect against myocardial damage and ventricular remodeling is related to changes in tenascin-C expression, and whether these really reflect the therapeutic effect, are also required.

In the present study, the anti–tenascin-C-antibody fragment was labeled so that the radioactivity would reveal inherent in vivo behaviors of the antibody fragment. The concordant spatial distribution of ^{125}I-TNC-Ab and immunohistochemical staining confirmed that the ^{125}I-TNC-Ab had bound to tenascin-C expressed in rat myocardium. Specific accumulation of ^{125}I-TNC-Ab in the myocardial area with ischemia and reperfusion was confirmed by a significantly lower accumulation of the nonspecific antibody in the area at risk.

For future clinical application as a SPECT agent, ^{123}I-TNC-Ab or ^{111}In-TNC-Ab is required. Labeling with ^{123}I can easily be performed in the same way as for ^{125}I, and ^{111}In labeling has already been achieved (*9,17*). Rapid blood clearance and retention of ^{125}I-TNC-Ab in the infarcted area, resulting in a decent target-to-blood ratio and good target-to-lung ratio, indicate the feasibility of in vivo imaging at 5 h or later after tracer injection. However, relatively high liver uptake resulted in a low target-to-liver ratio (0.66 at 5 h and 0.82 at 24 h), suggesting that careful interpretation might be required for myocardial uptake adjacent to the liver.

CONCLUSION

The present study demonstrated the feasibility of targeted ^{125}I-TNC-Ab imaging for serial assessment of regional expression of tenascin-C after myocardial ischemia and reperfusion. The study also demonstrated the spatiotemporal expression pattern after 20 and 30 min of ischemia and reperfusion. The data from this study implied that, by allowing visualization of tenascin-C expression, radiolabeled TNC Ab imaging may be a noninvasive way to monitor myocardial injury and its repair process after ischemia and reperfusion.

ACKNOWLEDGMENTS

This study was supported in part by 2 grants-in-aid for scientific research (C-20591437 and 19590813) from the Ministry of Education, Culture, Sports, Science, and Technology, Japan; by a research grant for intractable diseases from the Ministry of Health, Labor and Welfare of Japan; and by a grant from the Japan Foundation for the Promotion of the International Medical Center of Japan.

REFERENCES

1. White HD, Norris RM, Brown MA, Brandt PW, Whitlock RM, Wild CJ. Left ventricular end-systolic volume as the major determinant of survival after recovery from myocardial infarction. *Circulation.* 1987;76:44–51.
2. Chung CY, Murphy-Ullrich JE, Erickson HP. Mitogenesis, cell migration, and loss of focal adhesions induced by tenascin-C interacting with its cell surface receptor, annexin II. *Mol Biol Cell.* 1996;7:883–892.
3. Jones FS, Jones PL. The tenascin family of ECM glycoproteins: structure, function, and regulation during embryonic development and tissue remodeling. *Dev Dyn.* 2000;218:235–259.
4. Willems IE, Arends JW, Daemen MJ. Tenascin and fibronectin expression in healing human myocardial scars. *J Pathol.* 1996;179:321–325.
5. Imanaka-Yoshida K, Hiroe M, Nishikawa T, et al. Tenascin-C modulates adhesion of cardiomyocytes to extracellular matrix during tissue remodeling after myocardial infarction. *Lab Invest.* 2001;81:1015–1024.
6. Imanaka-Yoshida K, Hiroe M, Yasutomi Y, et al. Tenascin-C is a useful marker for disease activity in myocarditis. *J Pathol.* 2002;197:388–394.
7. Frangogiannis NG, Shimoni S, Chang SM, et al. Active interstitial remodeling: an important process in the hibernating human myocardium. *J Am Coll Cardiol.* 2002;39:1468–1474.
8. Morimoto S, Imanaka-Yoshida K, Hiramitsu S, et al. Diagnostic utility of tenascin-C for evaluation of the activity of human acute myocarditis. *J Pathol.* 2005;205:460–467.
9. Sato M, Toyozaki T, Odaka K, et al. Detection of experimental autoimmune myocarditis in rats by ^{111}In monoclonal antibody specific for tenascin-C. *Circulation.* 2002;106:1397–1402.
10. Tamura A, Kusachi S, Nogami K, et al. Tenascin expression in endomyocardial biopsy specimens in patients with dilated cardiomyopathy: distribution along margin of fibrotic lesions. *Heart.* 1996;75:291–294.
11. Tsukada B, Terasaki F, Shimomura H, et al. High prevalence of chronic myocarditis in dilated cardiomyopathy referred for left ventriculoplasty: expression of tenascin C as a possible marker for inflammation. *Hum Pathol.* 2009;40:1015–1022.

12. Hessel MH, Bleeker GB, Bax JJ, et al. Reverse ventricular remodelling after cardiac resynchronization therapy is associated with a reduction in serum tenascin-C and plasma matrix metalloproteinase-9 levels. *Eur J Heart Fail.* 2007;9:1058–1063.
13. Milting H, Ellinghaus P, Seewald M, et al. Plasma biomarkers of myocardial fibrosis and remodeling in terminal heart failure patients supported by mechanical circulatory support devices. *J Heart Lung Transplant.* 2008;27: 589–596.
14. Terasaki F, Okamoto H, Onishi K, et al; Study Group for Intractable Diseases by a Grant from the Ministry of Health, Labor and Welfare of Japan. Higher serum tenascin-C levels reflect the severity of heart failure, left ventricular dysfunction and remodeling in patients with dilated cardiomyopathy. *Circ J.* 2007;71:327–330.
15. Fujimoto N, Onishi K, Sato A, et al. Incremental prognostic values of serum tenascin-C levels with blood B-type natriuretic peptide testing at discharge in patients with dilated cardiomyopathy and decompensated heart failure. *J Card Fail.* 2009;15:898–905.
16. Sato A, Aonuma K, Imanaka-Yoshida K, et al. Serum tenascin-C might be a novel predictor of left ventricular remodeling and prognosis after acute myocardial infarction. *J Am Coll Cardiol.* 2006;47:2319–2325.
17. Odaka K, Uehara T, Arano Y, et al. Noninvasive detection of cardiac repair after acute myocardial infarction in rats by 111 In Fab fragment of monoclonal antibody specific for tenascin-C. *Int Heart J.* 2008;49:481–492.
18. Taki J, Higuchi T, Kawashima A, et al. Effect of postconditioning on myocardial ^{99m}Tc-annexin-V uptake: comparison with ischemic preconditioning and caspase inhibitor treatment. *J Nucl Med.* 2007;48:1301–1307.
19. Wilbur DS, Hadley SW, Grant LM, Hylarides MD. Radioiodinated iodobenzoyl conjugates of a monoclonal antibody Fab fragment: in vivo comparisons with chloramine-T-labeled Fab. *Bioconjug Chem.* 1991;2:111–116.
20. Kalembeyi I, Inada H, Nishiura R, Imanaka-Yoshida K, Sakakura T, Yoshida T. Tenascin-C upregulates matrix metalloproteinase-9 in breast cancer cells: direct and synergistic effects with transforming growth factor beta1. *Int J Cancer.* 2003; 105:53–60.
21. Nishiura R, Noda N, Minoura H, et al. Expression of matrix metalloproteinase-3 in mouse endometrial stromal cells during early pregnancy: regulation by interleukin-1alpha and tenascin-C. *Gynecol Endocrinol.* 2005;21:111–118.
22. Tamaoki M, Imanaka-Yoshida K, Yokoyama K, et al. Tenascin-C regulates recruitment of myofibroblasts during tissue repair after myocardial injury. *Am J Pathol.* 2005;167:71–80.

THE JOURNAL OF BIOLOGICAL CHEMISTRY VOL. 285, NO. 44, pp. 33680–33690, October 29, 2010

Heart-specific Small Subunit of Myosin Light Chain Phosphatase Activates Rho-associated Kinase and Regulates Phosphorylation of Myosin Phosphatase Target Subunit 1*

Received for publication, March 11, 2010, and in revised form, July 2, 2010 Published, JBC Papers in Press, August 27, 2010, DOI 10.1074/jbc.M110.122390

Daisuke Shichi[‡], Takuro Arimura[‡], Taisuke Ishikawa[‡], and Akinori Kimura[‡§1]

From the [‡]Department of Molecular Pathogenesis, Medical Research Institute, and the [§]Laboratory of Genome Diversity, School of Biomedical Science, Tokyo Medical and Dental University, Bunkyo-ku, Tokyo 113-8510, Japan

Phosphorylation of myosin regulatory light chain (MLC) plays a regulatory role in muscle contraction, and the level of MLC phosphorylation is balanced by MLC kinase and MLC phosphatase (MLCP). MLCP consists of a catalytic subunit, a large subunit (MYPT1 or MYPT2), and a small subunit. MLCP activity is regulated by phosphorylation of MYPTs, whereas the role of small subunit in the regulation remains unknown. We previously characterized a human heart-specific small subunit (hHS-M_{21}) that increased the sensitivity to Ca^{2+} in muscle contraction. In this study, we investigated the role of hHS-M_{21} in the regulation of MLCP phosphorylation. Two isoforms of hHS-M_{21}, hHS-M_{21}A and hHS-M_{21}B, preferentially bound the C-terminal one-third region of MYPT1 and MYPT2, respectively. Amino acid substitutions at a phosphorylation site of MYPT1, Ser-852, impaired the binding of MYPT1 and hHS-M_{21}. The hHS-M_{21} increased the phosphorylation level of MYPT1 at Thr-696, which was attenuated by Rho-associated kinase (ROCK) inhibitors and small interfering RNAs for ROCK. In addition, hHS-M_{21} bound ROCK and enhanced the ROCK activity. These findings suggest that hHS-M_{21} is a heart-specific effector of ROCK and plays a regulatory role in the MYPT1 phosphorylation at Thr-696 by ROCK.

Phosphorylation of myosin regulatory light chain (MLC)[2] plays pivotal roles in activation of actomyosin, regulation of cell shape, cell motility, and cytokinesis in eukaryotic cells (1–4). MLC phosphorylation is regulated by a balanced activity of two key enzymes: MLC phosphatase (MLCP) and MLC kinase (5). MLCP dephosphorylates the phosphorylated MLC, resulting in inactivation of myosin to cross-link actin filaments (6). It is well known that the MLC dephosphorylation induces Ca^{2+} desensitization of contractility, especially in the smooth muscle (6).

Many earlier works focused on MLCP in smooth muscle, and the current model for MLCP is based on the chicken gizzard MLCP (6). MLCP in smooth muscle is composed of a catalytic type 1 δ isoform (PP1cδ) subunit of ~38 kDa, a myosin phosphatase target subunit (MYPT) of ~110 kDa, and a small subunit of ~20 kDa (sm-M20) (6). PP1cδ required MYPT to interact with specific substrates at precise cellular localizations, and there are two isoforms of MYPT, MYPT1 and MYPT2. MYPT1 distributes ubiquitously in various tissues (7), whereas MYPT2 is mainly expressed in striated muscle and brain (8). MYPT1 and MYPT2 have common structural features as follows: ankyrin repeats in the N-terminal half and leucine zipper (LZ) motif in the C-terminal part. It was reported that both MYPT1 and MYPT2 formed a complex with PP1cδ and other molecules, such as moesin, microtubule-associated protein Tau, and MAP2, at the ankyrin repeats (9, 10). The C-terminal part of MYPT functions as a scaffold of substrates for several kinases and signal proteins, including small GTPase RhoA (11).

There are several mechanisms proposed for the regulation of MLCP activity, and the phosphorylation and dephosphorylation of MYPT were recognized as a major regulatory mechanism (12). Rho-associated kinase (ROCK), which belongs to a family of serine/threonine kinase and is activated by small GTPase RhoA, is known as a primary regulator of MYPT (13), and ROCK phosphorylates MYPT1 at threonine 696 (Thr-696) and threonine 853 (Thr-853) (numbering according to the human isoform) (12). Because MYPT2 contains equivalent phosphorylation sites (Thr-646 and Thr-808), it may also be regulated by the phosphorylation similar to MYPT1 (14). In addition, several other kinases, such as zipper-interacting protein kinase (ZIPK) and p21-activated kinase, are able to phosphorylate Thr-696 of MYPT1 (15, 16). Phosphorylation of MYPT1 at either Thr-696 or Thr-853 inhibited the MLCP activity and increased the sensitivity to Ca^{2+} of muscle contraction in smooth muscle (17). On the other hand, only limited information is available for the MLCP small subunit. The sm-M20 was characterized only in chicken gizzard, and it could bind the C-terminal part of MYPT1. However, it was reported that the binding of sm-M20 and MYPT1 did not affect the MLCP activity (6). It was demonstrated that sm-M20 increased

* This work was supported in part by grants-in-aid from the Ministry of Education, Culture, Sports, Science and Technology, Japan, grants for Japan-France collaboration research and Japan-Korea collaboration research from the Japan Society for the Promotion of Science, research grants from the Ministry of Health, Labour, and Welfare, Japan, grants from the Program for Promotion of Fundamental Studies in Health Sciences of the National Institute of Biomedical Innovation, Grant 11737 from the "Association Francaise Contre les Myopathies," a research grant for young investigators from Medical Research Institute, Tokyo Medical and Dental University, research grants from the Institute of Life Science, and by follow-up grants provided from the Tokyo Medical and Dental University.

The nucleotide sequence(s) reported in this paper has been submitted to the GenBank™/EBI Data Bank with accession number(s) AB588820.

[1] To whom correspondence should be addressed. Tel.: 81-3-5803-4905; Fax: 81-3-5803-4907; E-mail: akitis@mri.tmd.ac.jp.

[2] The abbreviations used are: MLC, myosin regulatory light chain; MLCP, MLC phosphatase; hHS-M_{21}, human heart-specific small subunit; MYPT, myosin phosphatase target subunit; ROCK, Rho-associated kinase; co-IP, co-immunoprecipitation; WB, Western blot; M2H, mammalian two-hybrid; aa, amino acid; ERM, ezrin/radixin/moesin; ZIPK, zipper-interacting protein kinase; LZ, leucine zipper; AU, arbitrary unit; Ab, antibody; pAB, polyclonal antibody.

the Ca^{2+} sensitivity of the contractile apparatus in vascular smooth muscle, the effect of which was conferred by the N-terminal half of sm-M20 (18). However, little is known about the functional roles of the small subunit in the regulation of MLCP activity, especially in muscles other than smooth muscle, such as cardiac muscle.

We have previously isolated heart-specific 21-kDa isoforms of the small subunit from human cardiac muscle, designated as hHS-M_{21} (7). The hHS-M_{21} is encoded by the same gene for *MYPT2*, involving exons 14–25, and there are two isoforms, hHS-M_{21}A and hHS-M_{21}B, which differed by structures of LZ motif at the C-terminal end, generated by an alternative splicing of exon 24 (7). It was revealed that hHS-M_{21} augmented the contraction of permeabilized porcine renal artery and rat cardiomyocyte at a constant Ca^{2+} concentration and that the N-terminal half of hHS-M_{21} conferred this action. In addition, hHS-M_{21} bound the C-terminal one-third region of MYPT1 with high affinity, and it bound to the corresponding region of MYPT2 only to a small extent. These findings implied that hHS-M_{21} played a role in the regulation of MYPT, although it has been established that the sensitivity to Ca^{2+} concentration in cardiac muscle contraction is mainly regulated by the troponin complex.

We demonstrate here that hHS-M_{21} is a positive regulator of ROCK and involved in the MYPT phosphorylation. This is the first study suggesting a regulatory mechanism by which hHS-M_{21} activates ROCK and modulates MYPT1 phosphorylation at Thr-696 by ROCK.

EXPERIMENTAL PROCEDURES

Mammalian Two-hybrid (M2H) Assay—The cDNA fragments for MYPT1 corresponding to amino acids (aa) 1–344 (N-terminal one-third of MYPT1; MYPT1-A), aa 345–688 (middle one-third of MYPT1; MYPT1-M), and aa 689–1030 (C-terminal one-third of MYPT1; MYPT1-P) and for MYPT2 corresponding to aa 1–328 (N-terminal one-third of MYPT2; MYPT2-A), aa 329–656 (middle one-third of MYPT2; MYPT2-M), and aa 657–982 (C-terminal one-third of MYPT2; MYPT2-P) were obtained by PCR from total heart cDNA. The C-terminal one-third regions of MYPTs were further divided into two parts as follows: MYPT1-Pt1 (aa 689–877 of MYPT1) and MYPT1-Pt2 (aa 878–1030 of MYPT1) for MYPT1, and MYPT2-Pt1 (aa 657–783 of MYPT2) and MYPT2-Pt2 (aa 784–982 of MYPT2) for MYPT2. The cDNA fragments for hHS-M_{21} were hHS-M_{21}A and hHS-M_{21}B (two isoforms of hHS-M_{21}; aa 1–208 and 1–224, respectively), hHS-M_{21}-t1 (deletion of the LZ motif from hHS-M_{21}), hHS-M_{21}-t2 (N-terminal half of hHS-M_{21}), hHS-M_{21}-t3 (deletion of N-terminal 56 residues and LZ motif from hHS-M_{21}), hHS-M_{21}-t4 (C-terminal half of hHS-M_{21}A), hHS-M_{21}-t5 (C-terminal half of hHS-M_{21}B), hHS-M_{21}-o1 (N-terminal 56 residues of hHS-M_{21}), and hHS-M_{21}-o2 (deletion of N-terminal 56 residues from C-terminal half of hHS-M_{21}). These cDNAs for MYPT1, MYPT2, and hHS-M_{21} were obtained by PCR from the MYPT1, MYPT2, and hHS-M_{21} plasmids, respectively (7). A full-length cDNA fragment (aa 1–186) of human sm-M20 was amplified by RT-PCR from human uterus cDNA. The PCR products were cloned into pCRII (Invitrogen) and sequenced to confirm that no PCR errors were introduced, and the insert cDNAs were excised by digestion with BamHI and SalI (for hHS-M_{21}, sm-M20 and MYPT2, MYPT1-A, and MYPT1-M constructs) or SalI and NotI (for MYPT1-P, -Pt1, and -Pt2 constructs). Excised cDNA fragments were then cloned into pACT vector containing VP16 as a prey (for hHS-M_{21} and sm-M20 constructs) and the pBIND vector containing GAL4 as a bait (for MYPT constructs) (CheckMate mammalian two-hybrid system, Promega). Sequence of primers and PCR conditions are available upon request. M2H assays were performed using Dual-Luciferase reporter assay system (Promega) as described previously (19). Arbitrary units (AU) were expressed as *Firefly* luciferase activities corrected by *Renilla reniformis* luciferase activities to normalize the transfection efficiency.

Pulldown Assay—The cDNA fragments for hHS-M_{21} and sm-M20 were generated by PCR from VP16-tagged hHS-M_{21} and sm-M20 plasmids described above and cloned into the pcDNA4/HisMax vector (Invitrogen) to obtain hexahistidine (His_6)-tagged hHS-M_{21} and sm-M20. The cDNA fragments for MYPT1-Pt3 (aa 822–1002) and MYPT2-Pt3 (aa 775–954), which lacked the LZ motifs and contained the phosphorylation sites at Ser-852/Thr-853, were generated by PCR and cloned into the pACT vector. Pulldown assay was performed using a HIS buffer kit (GE Healthcare) according to the manufacturer's instructions. Briefly, COS-7 cells (2×10^6) were seeded onto 150-mm dishes 1 day before the transfection, and each construct (10 μg) was individually transfected into the cells with 12 μl of COSFectin lipid reagent (Bio-Rad) according to the manufacturer's instruction. After 72 h of transfection, cells were harvested in binding buffer (20 mM sodium phosphate, 500 mM NaCl, 20 mM imidazole, 1% Nonidet P-40) containing a protease inhibitor mixture (Sigma). Total protein concentration was measured by BCA protein assay (Pierce). To evaluate the expression levels of transfected VP16-tagged MYPT, aliquots of the cell lysates were subjected to SDS-PAGE and transferred to a membrane for Western blotting (WB) with primary mouse anti-VP16 monoclonal antibody (mAb) (1:100, Santa Cruz Biotechnology) and secondary rabbit anti-mouse IgG HRP-conjugated Ab (1:1000, Dako A/S). Equivalent amounts of VP16-tagged proteins were used in the experiments. Cell lysates containing His_6-tagged hHS-M_{21}/sm-M20 or VP16-tagged MYPT1/MYPT2 were mixed with each other, and incubated at 37 °C for 2 h to form a binding complex. Subsequently, the admixture was incubated with nickel-Sepharose™ 6 Fast Flow (GE Healthcare) overnight at 4 °C. After washing three times with binding buffer, bound proteins were eluted by binding buffer containing 500 mM imidazole. The eluted samples were subjected to the SDS-PAGE followed by the WB analysis. The membrane of WB was incubated with primary mouse anti-VP16 mAb or rabbit anti-His_6 polyclonal antibody (pAb) (1:100 each, Santa Cruz Biotechnology) and with secondary rabbit anti-mouse (for mAb) or mouse anti-rabbit (for pAb) IgG HRP-conjugated Ab (1:1000, Dako A/S). Signals were visualized by Immobilon Western chemiluminescent HRP substrate (Millipore) and analyzed in Luminescent Image Analyzer LAS-3000mini (Fujifilm). The densitometric intensities were measured by MultiGauge version 3.0 (Fujifilm).

To mimic the phosphorylation and dephosphorylation states at Ser-852 and Thr-853 of MYPT1, cDNA fragments for wild-type (WT) and mutant MYPT1 (mMYPT1s, aa 689–1002) con-

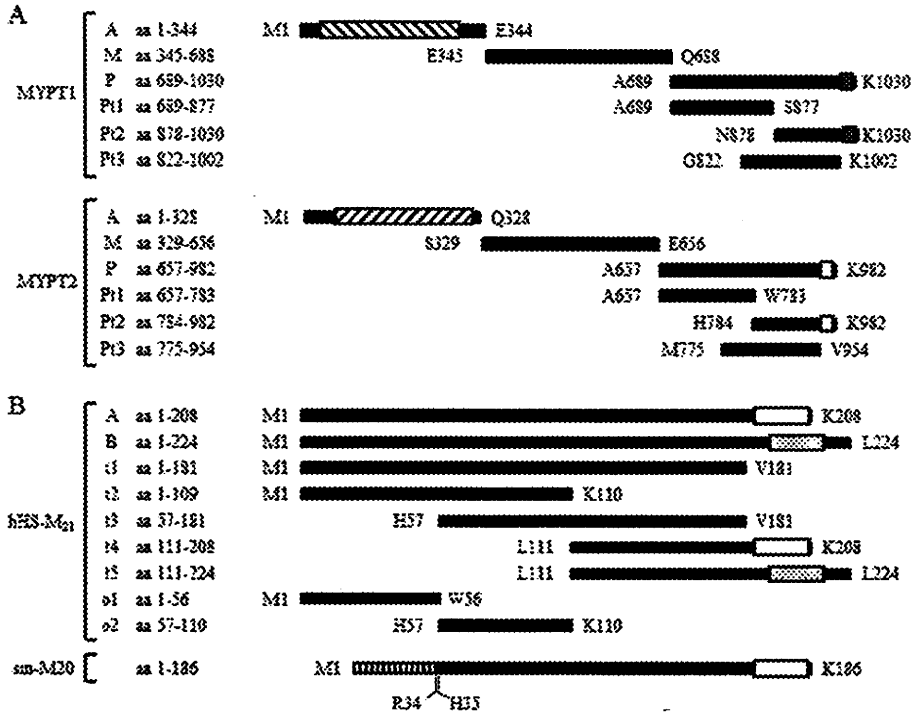

FIGURE 1. **Schematic representation of constructs used in M2H and pulldown assays.** Full-length and deletion mutants for large and small regulatory subunits of MLCP are schematically indicated along with their covering residues. *A*, constructs for myosin phosphatase target subunits (MYPT1 and MYPT2). *Diagonal hatched boxes* in the N terminus of MYPTs represent ankyrin repeats. *Shaded* and *open boxes* in the C terminus of MYPTs indicate LZ motifs of MYPT1 and MYPT2, respectively. *B*, constructs for MLCP small subunits (hHS-M_{21} and sm-M20). *Open* and *dotted boxes* in the C terminus of hHS-M_{21} indicate LZ motifs in hHS-M_{21}A and hHS-M_{21}B, respectively. C terminus of MYPT2 has identical sequences to that of hHS-M_{21}A and sm-M20. N-terminal 34 residues of sm-M20 (*vertical hatched box* of sm-M20) are different from that of hHS-M_{21}.

taining TCT to GAT (Ser-852 to Asp-852), TCT to GCT (Ser-852 to Ala-852), ACA to GAT (Thr-853 to Asp-853), or ACA to GCA (Thr-853 to Ala-853) were prepared where the substitutions were generated by the primer-directed mutagenesis method. Each mMYPT1 cDNA fragment was cloned into pACT to obtain VP16-tagged protein in transfection experiments. COS-7 cells (1×10^6) were seeded onto 100-mm dishes and co-transfected with a combination of pcDNA4/HisMax-hHS-M_{21}A constructs (4 μg) and pACT-mMYPT1 constructs (4 μg) with 9.6 μl of COSFectin lipid reagent. After 72 h of the transfection, cells were harvested, and the pulldown assay was performed as described above.

Phosphorylation Assay for MYPT1 and Ezrin/Radixin/Moesin (ERM)—The cDNA fragments for hHS-M_{21} were cleaved from pACT-hHS-M_{21}A, -hHS-M_{21}B, and -hHS-M_{21}-t1 plasmids and inserted into pCMV-Tag3 vector (Stratagene) to obtain Myc-tagged hHS-M_{21} in the transfection experiments. The cDNA fragments of full-length MYPT1 (major isoform in human heart; spliced out of exon 13) and constitutively active form of ROCK2 (ROCK2-act, aa 1–557) were amplified by RT-PCR from human heart cDNA and inserted into pcDNA3.1/Hygro(+) vector and pcDNA3.1/Zeo(+) vector, respectively. As for the MYPT1 phosphorylation assay, COS-7 (4×10^5) and HEK293 (8×10^5) cells were seeded onto 60-mm dishes and co-transfected with a combination of pcDNA3.1/Hygro full-length MYPT1 (2 μg) and pCMV-Tag3-hHS-M_{21} (0.1, 0.5, 1, and 2 μg) with 4.8 μl of COSFectin lipid reagent (for COS-7 cell) or 9 μl of TransFectin lipid reagent (for HEK293 cells, Bio-Rad). COS-7 cells were also co-transfected with pcDNA3.1/Hygro full-length MYPT1 (2 μg) alone, pcDNA3.1/Hygro full-length MYPT1 (2 μg) plus pcDNA3.1/Zeo-ROCK2-act (2 μg), or pcDNA3.1/Hygro full-length MYPT1 (2 μg) plus pcDNA3.1/Zeo-ROCK2-act (2 μg) plus pCMV-Tag3-hHS-M_{21} (2 μg), with 7.2 μl of COSFectin lipid reagent. As for the ERM phosphorylation assay, COS-7 cells (4×10^5) were seeded onto 60-mm dishes, and pCMV-Tag3-hHS-M21 (2 μg) or pcDNA3.1/Zeo-ROCK2-act (2 μg) was transfected using 2.4 μl of COSFectin lipid reagent. In some experiments, COS-7 cells were treated with a ROCK-specific inhibitor, Y-27632 (Sigma), or fasudil hydrochloride (Wako) at a final concentration of 20 μM before the transfection, when it was needed.

After 48 h of the transfection, cells were subjected to brief sonication in TNE buffer (1% Nonidet P-40, 1 mM EDTA, 150 mM NaCl, and 10 mM Tris-HCl, pH 7.8) containing a protease inhibitor mixture and phosphatase inhibitors (10 mM NaF and 2 mM Na_3VO_4). After measuring the protein concentration, equal amounts of proteins were subjected to SDS-PAGE and WB experiments. The following primary Abs were used: mouse anti-c-Myc mAb (1:100, Santa Cruz Biotechnology), rabbit anti-phospho-MYPT1-Thr-696 pAb (1:500), rabbit anti-phospho-MYPT1-Thr-853 pAb (1:350, Millipore), rabbit anti-MYPT1 pAb (1:100, Santa Cruz Biotechnology), rabbit anti-ROKα/ROCK2 pAb (1:500, Millipore), rabbit anti-ezrin/radixin/moesin pAb (1:500, Santa Cruz Biotechnology), and rabbit anti-phospho ezrin (Thr-567)/radixin (Thr-564)/moesin (Thr-558) pAb (1:250, Santa Cruz Biotechnology).

Inhibition Assay of ROCK Activity—COS-7 cells (4×10^5) were seeded onto 60-mm dishes, and 24 h later, a ROCK-specific inhibitor, Y-27632 (Sigma) or fasudil hydrochloride (Wako), was added at a final concentration of 1, 10, or 20 μM. Then pcDNA3.1/Hygro full-length MYPT1 (2 μg), pcDNA3.1/Hygro full-length MYPT1 (2 μg) plus pcDNA3.1/Zeo-ROCK2-act (2 μg), or pcDNA3.1/Hygro full-length MYPT1 (2 μg) plus pCMV-Tag3-hHS-M_{21} (2 μg) were transfected using COSFectin lipid reagent. Cells were cultured with Y-27632 or fasudil hydrochloride for 48 h and harvested in TNE buffer containing a protease inhibitor mixture and phosphatase inhibitors. Cell lysates were subjected to SDS-PAGE and WB analysis, as described above.

Silencing of Endogenous ROCK by Small Interfering RNA (siRNA)—Pre-designed siRNAs for human ROCK2 (siRNA ID, s18162 and s225145) and a nonsilencing siRNA as a negative

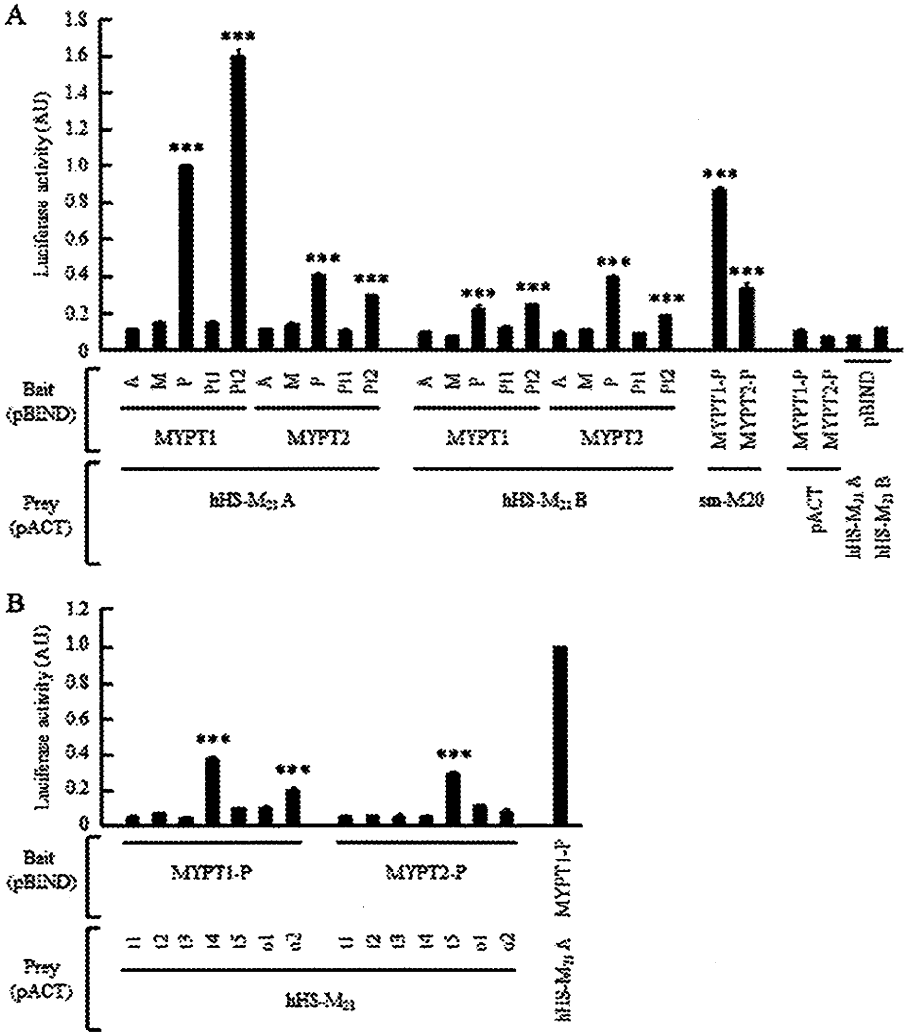

FIGURE 2. **M2H assay in evaluating the binding of hHS-M_{21}/sm-M20 with MYPTs.** Luciferase activities obtained in the M2H assay. *A*, binding pairs were deletion mutants of MYPT1 or MYPT2 with hHS-M_{21}A, hHS-M_{21}B, or sm-M20. pACT and pBIND indicate transfection with pACT or pBIND vectors, respectively, as controls (no VP16- and GAL4-tagged proteins). *B*, binding pairs were deletion mutants of hHS-M_{21}A or hHS-M_{21}B with MYPT1-P or MYPT2-P. Data for MYPT1-P with hHS-M_{21}A were arbitrarily defined as 1.00 AU. Data are represented as means ± S.E. ($n = 3$ for control or $n = 4$ for each case). ***, $p < 0.001$ *versus* controls.

control were obtained from Ambion (Austin). COS-7 cells (2×10^5) were seeded onto 60-mm dishes and transfected with siRNAs at a final concentration of 5 nM using Lipofectamine 2000 (Invitrogen). After 24 h of the treatment with siRNAs, pcDNA3.1/Hygro full-length MYPT1 (2 μg) and pCMV-Tag3-hHS-M_{21} (2 μg) were co-transfected into the siRNA-transfected cells. After 48 h of the initial siRNA transfection, each siRNA (5 nM) was transfected into the cells. After an additional 24 h, cells were harvested and subjected to the SDS-PAGE and WB analysis. The primary Abs used for WB were as follows: mouse anti-c-Myc mAb (1:100), rabbit anti-phospho-MYPT1 Thr-696 pAb (1:500), rabbit anti-MYPT1 pAb (1:100), rabbit anti-ROKα/ROCK2 pAb (1:500), and mouse anti-GAPDH mAb (1:100, Santa Cruz Biotechnology).

Co-immunoprecipitation (Co-IP) Assay—The cDNA fragment for full-length MYPT1 was inserted into pCMV-Tag2 vector (Stratagene) to obtain FLAG-tagged full-length MYPT1. COS-7 cells (1×10^6) were seeded onto 100-mm dishes, and either pCMV-Tag3-hHS-M_{21} (4 μg) or pCMV-Tag2-full-length MYPT1 (4 μg) alone or both were transfected using COSFectin lipid reagent. After 48 h of the transfection, cells were harvested, and co-IP assay was performed as described previously (20). Cell lysates were incubated with 4 μg of control mouse IgG (Caltag Laboratories), mouse anti-c-Myc mAb, or mouse anti-FLAG mAb (Sigma) for co-IP. The primary Abs used for WB were as follows: mouse anti-c-Myc mAb (1:100), mouse anti-FLAG mAb (1:250), and rabbit anti-ROKα/ROCK2 pAb (1:500).

Statistical Analysis—Numerical data were expressed as means ± S.E. Statistical differences were analyzed using Tukey's multiple comparison tests. Statistical analyses were performed using the *R* statistical computing environment version 2.6.1. *p* values less than 0.05 were considered to be statistically significant.

RESULTS

Analysis of Binding Domains in hHS-M_{21} and MYPTs—We first characterized a human equivalent isoform of sm-M20 that had been characterized only in chicken gizzard (21). It was suggested that the N-terminal end of human sm-M20 would be encoded within intron 18 of the gene for *MYPT2*, whereas the C-terminal residues were translated from the following exons (7, 22). Because we found a region homologous to 5′ side of avian sm-M20 cDNA in intron 18, which was 18.6-kbp upstream of exon 19, this information was used to design a 5′-sided primer to isolate a full-length sm-M20 by RT-PCR. It was demonstrated that human sm-M20 consisted of 186-aa residues, and the N-terminal side (aa 1–34) differed from the N-terminal side of MYPT2 and hHS-M_{21} (Fig. 1). It was found that exon 24 was not alternatively spliced in encoding the cDNA for sm-M20 (human sm-M20 cDNA sequence was submitted to DDBJ and given an accession no. AB588820). Expression analysis of sm-M20 in various human tissues by RT-PCR showed a high level expression in the tissues abundant with smooth muscle, including uterus, small intestine, and colon, whereas a weak expression and no expression were observed in skeletal muscle and heart, respectively (data not shown).

To determine the binding domains in hHS-M_{21} and MYPTs, we first performed M2H assay. A bait construct containing each

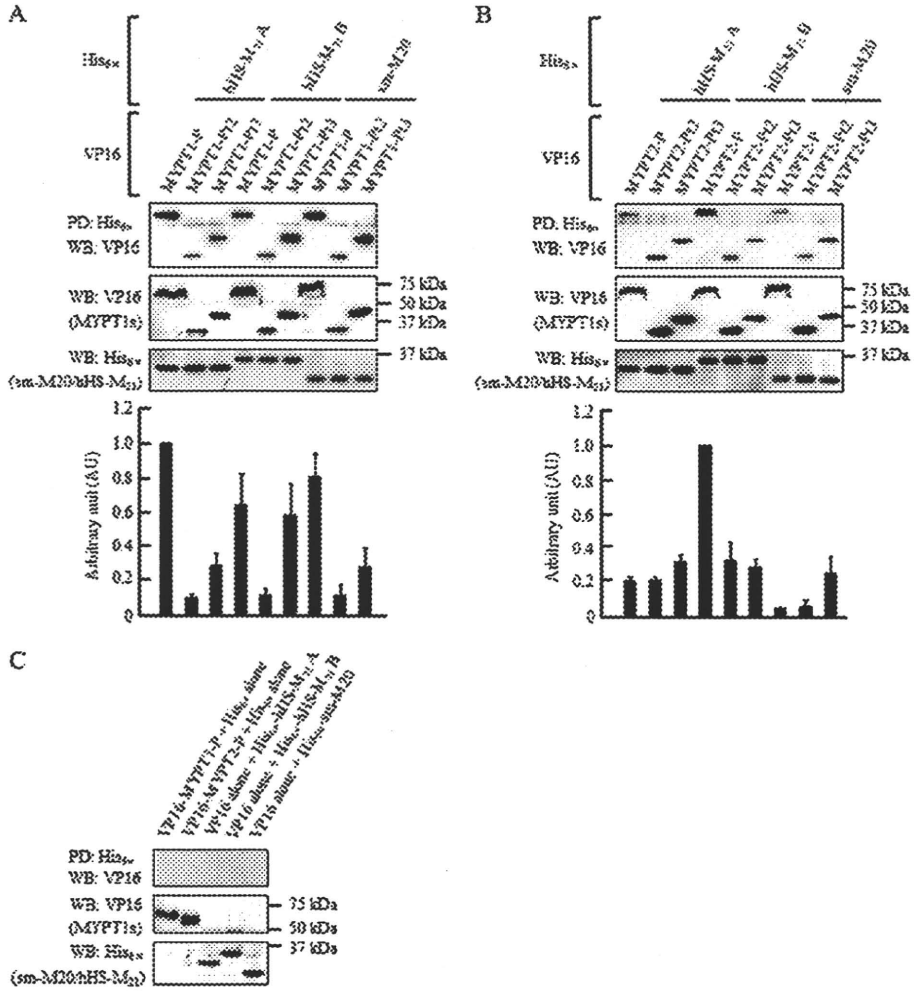

FIGURE 3. **Pulldown assay for binding of hHS-M_{21}/sm-M20 with C terminus of MYPT1 or MYPT2.** Binding of hHS-M_{21}A, hHS-M_{21}B, or sm-M20 with MYPT1 (*A*) or MYPT2 (*B*) was analyzed. VP16-tagged MYPT1-P or -MYPT2-P was pulled down (*PD*) with His_6-tagged hHS-M_{21}A, -hHS-M_{21}B, or -sm-M20 and detected by using anti-VP16 Ab. Expression levels of VP16-tagged MYPTs and His_6-tagged small subunits were evaluated by immunoblotting of whole-cell lysates. Densitometric data obtained in the pulldown assays are shown in *lower panel*. *Bars* indicate the amounts of pulldown products normalized to the amount of input VP16-MYPTs. Data for VP16-MYPT1-P with His_6-hHS-M_{21}A (*A*) or VP16-MYPT2-P with His_6-hHS-M_{21}B (*B*) were arbitrarily defined as 1.00 AU. Data are represented as means ± S.E. ($n = 5$ for each case). *C*, VP16-tagged MYPT1s pulled down with His_6 protein alone or VP16 protein alone pulled down with His_6-tagged small subunits were not detected.

one-third of MYPTs was co-transfected with a prey construct for hHS-M_{21} or sm-M20 (Fig. 1), and luciferase activities in co-transfectants were measured. When the luciferase activity in the transfectants with hHS-M_{21}A plus MYPT1-P was arbitrarily defined as 1.00 AU, that of hHS-M_{21}A plus MYPT2-P showed a significant binding (0.40 ± 0.01 AU, $p < 0.001$, as compared with negative controls containing either MYPTs or hHS-M_{21} construct alone), and those of hHS-M_{21}B plus MYPTs were 0.21 ± 0.01 or 0.39 ± 0.01 AU for MYPT1-P or MYPT2-P, respectively ($p < 0.001$ in each case), indicating that both isoforms of hHS-M_{21} could interact with the C-terminal one-third of MYPTs (MYPT1-P and MYPT2-P) (Fig. 2*A*), as reported previously by using an overlay assay (7). In addition, hHS-M_{21}A preferentially bound MYPT1-P, whereas hHS-M_{21}B preferentially bound MYPT2-P (Fig. 2*A*). It should be noted that sm-M20, which differed from hHS-M_{21}A only at the N-terminal part (aa 1–34), bound both MYPT1-P and MYPT2-P, and the luciferase activities in the transfectants with sm-M20 plus MYPTs were similar to that of hHS-M_{21} plus MYPTs (Fig. 2*A*).

Next, the hHS-M_{21}-binding site in the C-terminal one-third of MYPTs was analyzed using MYPT1-Pt1, MYPT1-Pt2, MYPT2-Pt1, and MYPT2-Pt2 (Fig. 1*A*). As shown in Fig. 2*A*, luciferase activities in the transfectants containing hHS-M_{21}A or hHS-M_{21}B with MYPT1-Pt2 (1.61 ± 0.03 or 0.24 ± 0.01 AU, respectively) or with MYPT2-Pt2 (0.29 ± 0.01 or 0.18 ± 0.01 AU, respectively) were significantly higher than those of the negative controls ($p < 0.001$ for each case), demonstrating that the C-terminal end of MYPTs (aa 878–1030 of MYPT1 and aa 784–982 of MYPT2) possessed a binding site for hHS-M_{21}. In addition, we analyzed the MYPT-binding site in the deletion mutant of hHS-M_{21} (Fig. 1*B*). Luciferase activities in the transfectants containing hHS-M_{21}-t4 plus MYPT1-P and hHS-M_{21}-t5 plus MYPT2-P were significantly higher (0.37 ± 0.01 and 0.28 ± 0.01 AU, respectively, $p < 0.001$ for each case) than the negative controls (Fig. 2*B*), suggesting that the C-terminal half of hHS-M_{21}A preferentially bound MYPT1, whereas that of hHS-M_{21}B preferentially bound MYPT2.

To confirm and further investigate the binding between hHS-M_{21} and MYPTs, we performed a pull-down assay. Consistent with the M2H data showing the interaction between the C-terminal one-third of MYPT1 (MYPT1-P) and MLCP small subunits (hHS-M_{21}A, hHS-M_{21}B, and sm-M20), WB analysis of pulldown products from the mixture of cell lysates prepared from transfectants of VP16-MYPT1-P in combination with His_6-hHS-M_{21}A, -hHS-M_{21}B, or -sm-M20 revealed that the C-terminal one-third of MYPT1 could bind all isoforms of the MLCP small subunit (Fig. 3*A*). To map the binding site in MYPT1, VP16-MYPT1-Pt2 (aa 878–1030) and VP16-MYPT1-Pt3 (aa 822–1002) were tested for pulldown with His_6-hHS-M_{21}A, -hHS-M_{21}B, or -sm-M20. As shown in Fig. 3*A*, the MYPT1 series were pulled down, and the interaction of the small subunits with MYPT1-Pt3 was higher than that with MYPT1-Pt2, suggesting that the LZ motif of MYPT1 was not a major binding motif, whereas the region around the phosphorylation site of MYPT1 at Thr-853 might be a binding domain for the small subunits. WB analysis of

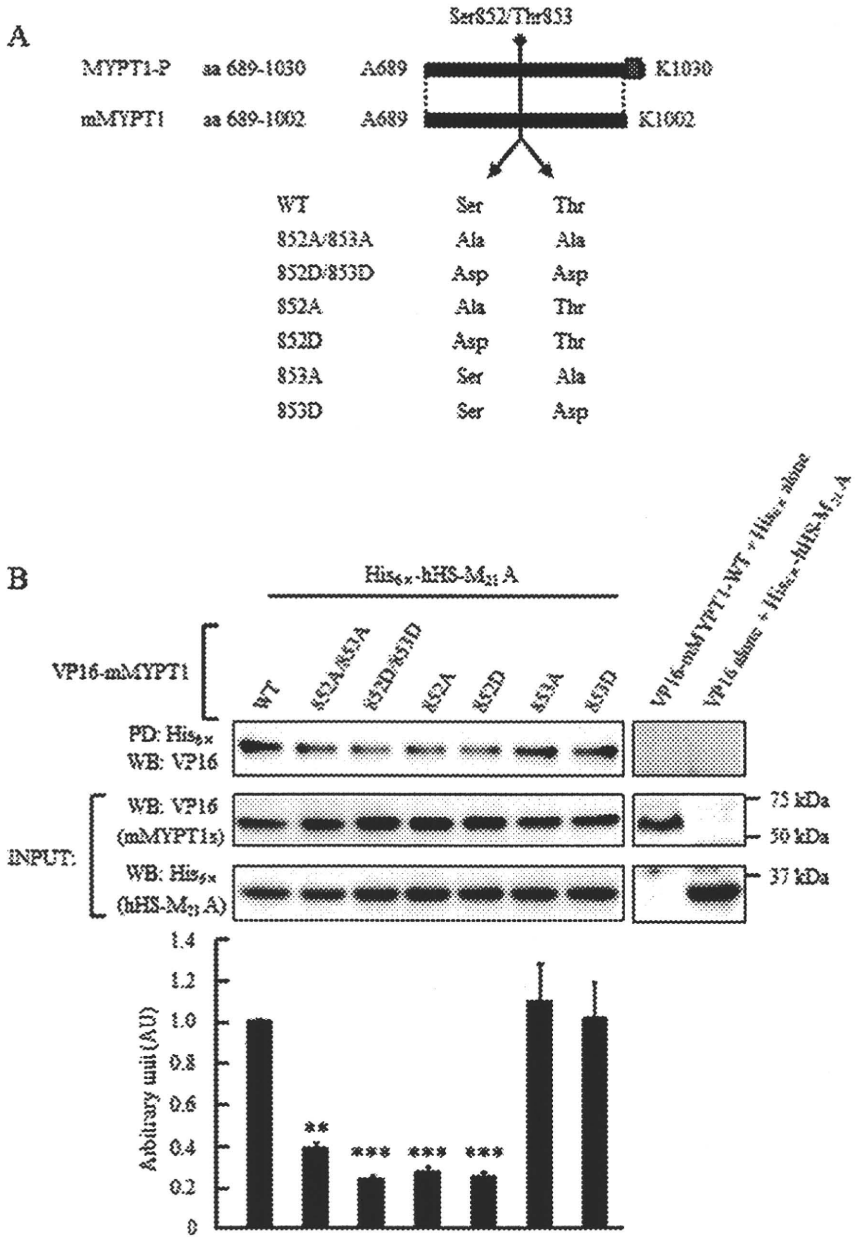

FIGURE 4. **Binding of hHS-M_{21} and MYPT1 in mimicking phosphorylation or dephosphorylation status at Ser-852/Thr-853.** *A*, schematic structures of wild-type (*WT*) and mutant MYPT1 (*mMYPT1*) truncated the LZ motif from MYPT1-P. Nonphosphorylatable (Ala) and/or phosphorylation-mimicking (Asp) substitutions at Ser-852 and Thr-853 within mMYPT1 are indicated. *B*, binding of hHS-M_{21}A and MYPT1 with or without the substitutions at Ser-852/Thr-853. VP16-mMYPT1s pulled down (*PD*) with His_6-hHS-M_{21}A were detected by using anti-VP16 Ab. Expression levels of VP16-MYPTs and His_6-hHS-M_{21}A were evaluated by immunoblotting of whole-cell lysates. Densitometric data obtained in the pulldown assay are shown in the *lower panel*. *Bars* indicate the amounts of pulldown products normalized to the amounts of VP16-mMYPT1s. Data for VP16-mMYPT1-WT with His_6-hHS-M_{21}A were arbitrarily defined as 1.00 AU. Data are represented as means ± S.E. (n = 5 for each case). **, $p < 0.01$; ***, $p < 0.001$ *versus* WT.

pulldown products from lysates of His_6-tagged small subunits with VP16-MYPT2-P, -Pt2, or -Pt3 also confirmed the binding of the small subunits with the C-terminal one-third of MYPT2. As was shown in the M2H assay, hHS-M_{21}B bound MYPT2-P stronger than hHS-M_{21}A and sm-M20 (Fig. 3*B*).

Binding of MYPT1 with hHS-M_{21} under Mimicking Phosphorylation/Dephosphorylation Status at Ser-852/Thr-853—Because the possible binding domain of MYPT1 for the small subunits contains two phosphorylation sites at Thr-853 and Ser-852, which is phosphorylated by protein kinase A/G and/or ROCK (23, 24), we investigated whether the phosphorylation status of MYPT1 at these sites would affect the binding between the C-terminal MYPT1 and hHS-M_{21}A. We generated VP16-tagged MYPT1 (aa 689–1002) of WT or mutants (mMYPT1), in which Ser-852 and/or Thr-853 phosphorylation sites were replaced by nonphosphorylatable (Ala) or phosphorylation-mimicking (Asp) residues (Fig. 4*A*) to be used in the pulldown assay. As shown in Fig. 4*B*, binding of hHS-M_{21}A with mMYPT1–853A or -853D was not significantly different from that with mMYPT1-WT. In clear contrast, mMYPT1–852A/853A, -852D/853D, -852A, and -852D bound hHS-M_{21}A significantly less (0.39 ± 0.02, 0.24 ± 0.02, 0.28 ± 0.01, and 0.25 ± 0.02 AU, respectively, $p <$ 0.01 for each case) than WT (defined as 1.00 AU) (Fig. 4*B*). These data indicated that the substitutions at Ser-852, irrespective of mimicking the phosphorylation/dephosphorylation status, affected the binding of mMYPT1 and hHS-M_{21}A, whereas the phosphorylation status of mMYPT1 at Thr-853 was suggested not to change the binding.

Regulation of Phosphorylation at Thr-696 of MYPT1 by hHS-M_{21}—To investigate the functional role of hHS-M_{21} in the regulation of the phosphorylation/dephosphorylation status of MYPT1, nontagged MYPT1 was co-transfected with Myc-tagged hHS-M_{21}A, hHS-M_{21}B, or hHS-M_{21}-t1 into COS-7 cells. WB analyses of the lysates from the co-transfected cells using antibodies against MYPT1-Thr(P)-696 or -Thr(P)-853 demonstrated a 1.8-fold increase of phosphorylation at Thr-696 ($p < 0.001$) in the presence of hHS-M_{21}A, whereas Thr(P)-853 level was not altered by the co-expression of hHS-M_{21}A (Fig. 5, *A* and *B*). In addition, the phosphorylation level of MYPT1 at Thr-696 was increased depending on the amounts of co-expressed hHS-M_{21}A (Fig. 5, *C* and *D*). In clear contrast, expression of hHS-M_{21}B or hHS-M_{21}-t1 did not change the phosphorylation level of MYPT1 at both Thr-696 and Thr-853. Because the increased

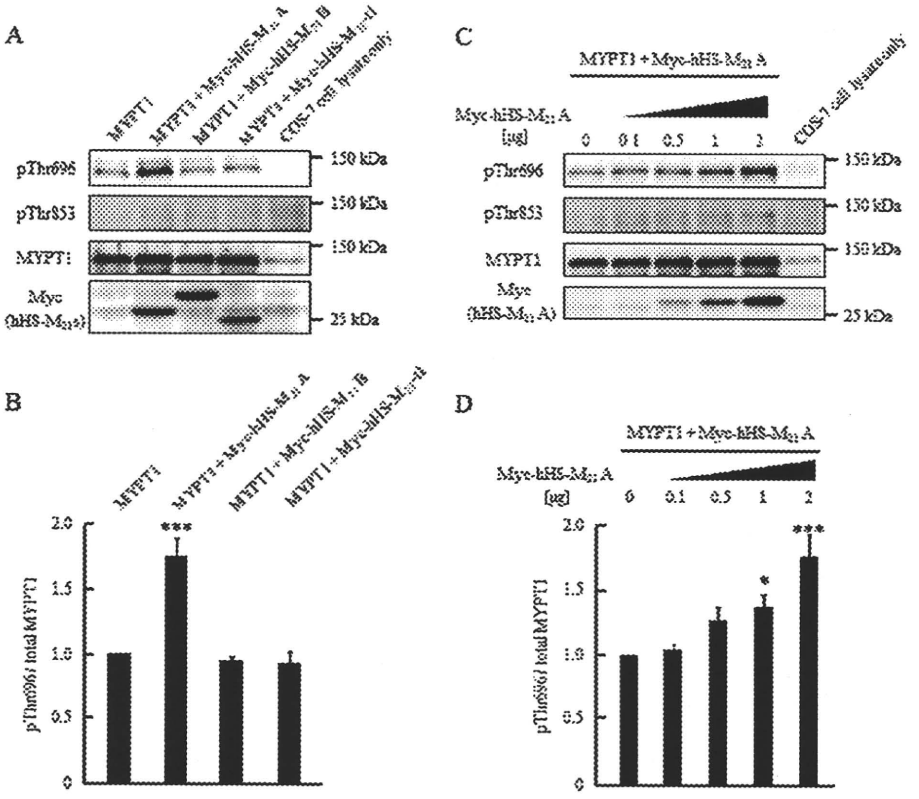

FIGURE 5. **MYPT1 phosphorylation at Thr-696 and Thr-853 in the presence of hHS-M_{21}.** *A*, amounts of MYPT1 phosphorylation level in COS-7 cells transfected with nontagged MYPT1 alone (2 μg) or in the combination of nontagged MYPT1 (2 μg) and Myc-tagged hHS-M_{21} (2 μg) (referred to in Fig. 1*B*) were measured by using anti-phospho-MYPT1-Thr-696 (*pThr696*) or -Thr-853 (*pThr853*) Abs. Expression levels of MYPT1 and Myc-hHS-M_{21} were evaluated by immunoblotting of whole-cell lysates. *B*, densitometric analysis of MYPT1-Thr(P)-696 blotting data in *A*. *Bars* indicate the Thr(P)-696 phosphorylation levels normalized to the amounts of total MYPT1. Data for MYPT1 without Myc-hHS-M_{21} was arbitrarily defined as 1.00 AU. Data are represented as means ± S.E. (n = 5 for each case). ***, $p < 0.001$ *versus* MYPT1 without Myc-hHS-M_{21}. *C*, MYPT1 phosphorylation at Thr-696 in the cells transfected with nontagged MYPT1 (2 μg) in combination of Myc-tagged hHS-M_{21}A (0, 0.1, 0.5, 1, and 2 μg). *D*, densitometric analysis of MYPT1-Thr(P)-696 blotting data in *C*. *Bars* indicate the Thr-696 phosphorylation levels normalized to the amounts of total MYPT1. Data for MYPT1 without Myc-hHS-M_{21} were arbitrarily defined as 1.00 AU. Data are represented as means ± S.E. (n = 5 for each case). *, $p < 0.05$; ***, $p < 0.001$ *versus* MYPT1 without Myc-hHS-M_{21}.

phosphorylation of MYPT1 at Thr-696 regulated by hHS-M_{21}A might be specific to COS-7 cells, we examined HEK293 cells co-transfected with nontagged MYPT1 plus Myc-tagged hHS-M_{21}A. We obtained essentially the same results of increased phosphorylation of MYPT1 at Thr-696 in the presence of hHS-M_{21}A (data not shown). These findings suggested that hHS-M_{21}A specifically regulated the phosphorylation of MYPT1 at Thr-696 and that the LZ motif of hHS-M_{21}A played a role in the regulation, because such effects were not observed for hHS-M_{21}B or hHS-M_{21}-t1 lacking the LZ motif.

Effect of ROCK on the Phosphorylation of MYPT1 Regulated by hHS-M_{21}—It has been reported that ROCK phosphorylates MYPT1 at two different phosphorylation sites, Thr-696 and Thr-853 (24, 25), which lead to inhibition of MLCP activity (17, 26). More recently, it was demonstrated that aa 683–866 of MYPT1 was a minimal binding domain of ROCK (27). Because the binding region of MYPT1 with hHS-M_{21}A identified in this study appeared similar to that with ROCK, we hypothesized that ROCK might functionally interact with hHS-M_{21}A in the phosphorylation of MYPT1. We investigated the effect of two ROCK-specific inhibitors, Y-27632 and fasudil, on the phosphorylation levels of MYPT1 at Thr-696 and Thr-853 in the presence of hHS-M_{21}A. COS-7 cells transfected with nontagged MYPT1 alone or co-transfected with nontagged MYPT1 plus Myc-tagged hHS-M_{21}A were treated with Y-27632 or fasudil at the concentrations of 1, 10, and 20 μM, and subjected to the WB analyses. It was demonstrated that the treatments with Y-27632 and fasudil inhibited the increased phosphorylation of MYPT1 at Thr-696 regulated by Myc-hHS-M_{21}A and that the inhibition was in a dose-dependent manner and specific to the phosphorylation status, because the treatment with Y-27632 or fasudil showed no significant effect on the expression levels of MYPT1, hHS-M_{21}A, and endogenous ROCK (Fig. 6, *A* and *B*).

To evaluate the involvement of ROCK in the regulation of MYPT1 phosphorylation at Thr-696 by hHS-M_{21}A, ROCK was silenced by using two pre-designed siRNAs (s18162 and s225145) in COS-7 cells co-transfected with nontagged MYPT1 and Myc-tagged hHS-M_{21}A. The amount of targeted ROCK protein was decreased by ~72% or 86% with s18162 or s225145, respectively, as compared with that with control siRNA (Fig. 7*A*). Silencing of ROCK by the siRNA, s18162 or s225145, caused significant reduction in the phosphorylation status of MYPT1 at Thr-696 ($p < 0.001$ for each case *versus* control siRNA) regulated by hHS-M_{21}A, whereas the knocking down of endogenous ROCK did not affect the expression of MYPT1 and Myc-hHS-M_{21}A (Fig. 7*B*). These data suggested that hHS-M_{21}A regulated the phosphorylation at Thr-696 of MYPT1 through ROCK.

Interaction among ROCK, MYPT1, and hHS-M_{21}—It was reported that MYPT1 bound both ROCK (27) and hHS-M_{21}A (7). To further investigate the interaction among them, FLAG-tagged MYPT1 and Myc-tagged hHS-M_{21} were individually immunoprecipitated using anti-FLAG or -Myc Ab from COS-7 cells transfected with FLAG-MYPT1 or Myc-hHS-M_{21}A alone. WB analysis of immunoprecipitates from the transfectants revealed that endogenous ROCK bound both FLAG-MYPT1 and Myc-hHS-M_{21} (Fig. 8). We also co-transfected FLAG-MYPT1 and Myc-hHS-M_{21}A into COS-7 cells. It was found that the binding of endogenous ROCK with FLAG-MYPT1 or Myc-hHS-M_{21}A was not altered in the presence of Myc-hHS-

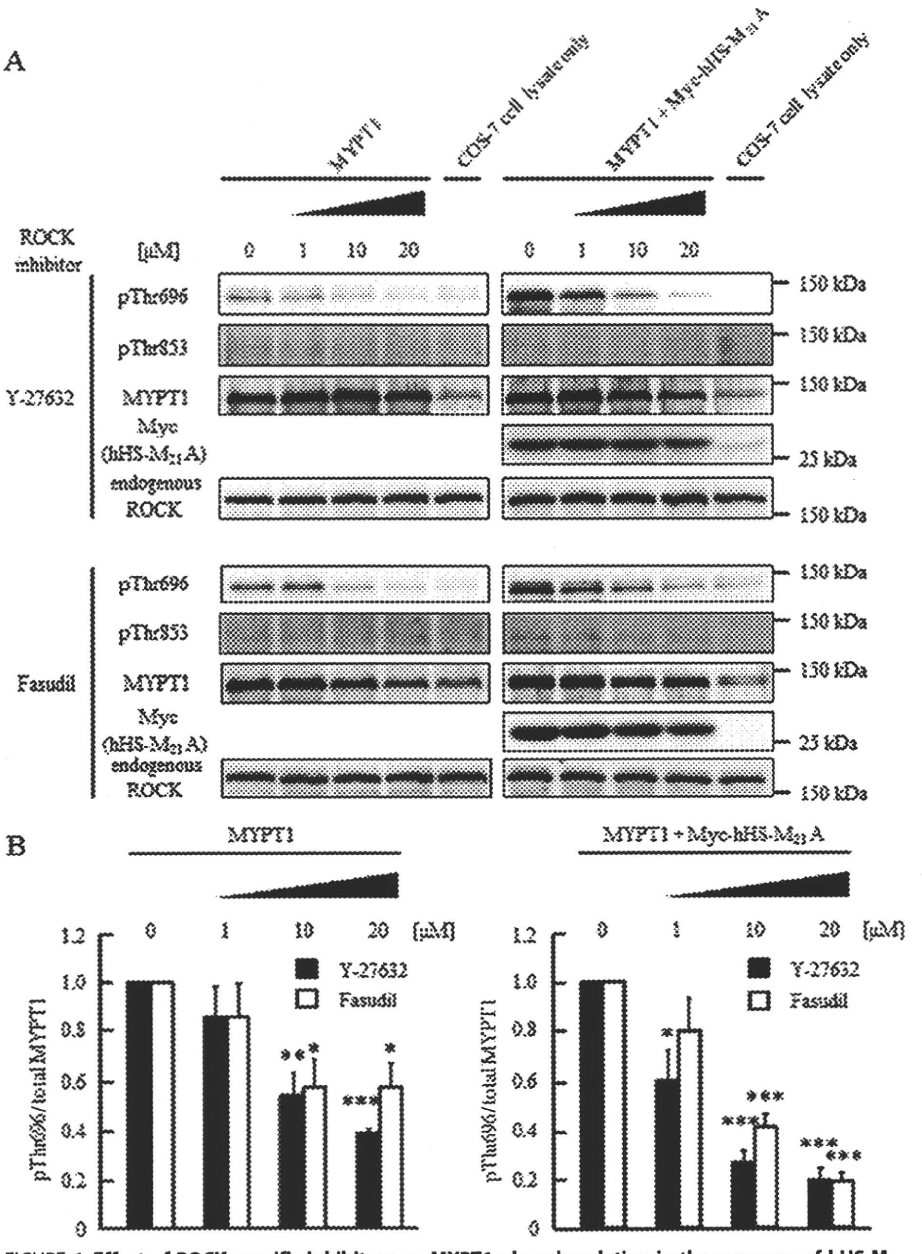

FIGURE 6. **Effect of ROCK-specific inhibitors on MYPT1 phosphorylation in the presence of hHS-M_{21}.** *A*, COS-7 cells co-transfected with nontagged MYPT1 alone (*left panel*) or nontagged MYPT1 plus Myc-tagged hHS-M_{21}A (*right panel*) were treated with ROCK-specific inhibitor, Y-27632 (0, 1, 10, and 20 μM; *upper panel*) or fasudil (0, 1, 10, and 20 μM; *lower panel*). MYPT1 phosphorylation level was measured by using anti-phospho-MYPT1-Thr-696 (*pThr696*) or -Thr-853 (*pThr853*) Abs. Expression levels of MYPT1, Myc-hHS-M_{21}A, and endogenous ROCK were evaluated by immunoblotting of whole-cell lysates. *B*, densitometric analysis of MYPT1-Thr(P)-696 blotting data in *A*. *Bars* indicate the Thr-696 phosphorylation levels normalized to the amounts of total MYPT1. Data for without Y-27632 or fasudil were arbitrarily defined as 1.00 AU. Data are represented as means ± S.E. ($n = 5$ for each case). *, $p < 0.05$; **, $p < 0.01$; ***, $p < 0.001$ *versus* no treatment with Y-27632 or fasudil.

M_{21}A or FLAG-MYPT1, respectively (Fig. 8), suggesting that hHS-M_{21}A and MYPT1 formed a trimetric complex with ROCK.

Effect of hHS-M_{21} on the Phosphorylation of MYPT1 Regulated by ROCK—To evaluate the effect of hHS-M_{21} in the regulation of MYPT1 phosphorylation at Thr-696 and Thr-853 by ROCK, we examined COS-7 cells transfected with nontagged MYPT1 alone, co-transfected nontagged MYPT1 plus nontagged ROCK2-act, or nontagged MYPT1 plus nontagged ROCK2-act plus Myc-hHS-M_{21}A. WB analyses of lysates from co-transfected cells using antibodies against MYPT1-Thr(P)-696 or -Thr(P)-853 showed that the phosphorylation at both Thr-696 and Thr-853 was significantly increased in the presence of ROCK2-act (Fig. 9). The phosphorylation level of MYPT1 at Thr-696 was further increased by the presence of Myc-hHS-M_{21}A with ROCK2-act (Fig. 9, *A* and *B*). Interestingly, the increased phosphorylation level of MYPT1 at Thr-853 by ROCK2-act was significantly suppressed by Myc-hHS-M_{21}A (Fig. 9, *A* and *C*), suggesting that Myc-hHS-M_{21}A had an inhibitory effect on the phosphorylation at Thr-853 but not at Thr-696 of MYPT1 by ROCK.

Regulation of ERM Phosphorylation by hHS-M_{21}—Because hHS-M_{21} might increase ROCK activity, we investigated the phosphorylation level of another substrate of ROCK, endogenous ERM (28). WB analyses of lysates from transfected COS-7 cells using antibodies against phospho-ERM demonstrated a 1.9-fold increase of ERM phosphorylation in the presence of hHS-M_{21}A, and the phosphorylation was specifically attenuated by the ROCK inhibitor (Fig. 10), suggesting that ROCK was activated by hHS-M_{21}A.

DISCUSSION

Ca^{2+} plays a central role in the regulation of the muscle contractile process mediated by the interaction of myosin with actin. In the smooth muscle, the phosphorylation status of MLC is correlated with the Ca^{2+} sensitivity of muscle contraction (13). By contrast, in the cardiac muscle, it is well known that the Ca^{2+} sensitivity of muscle contraction is mainly regulated by the troponin complex, and the significance of MLC phosphorylation in Ca^{2+} sensitization is not fully elucidated. It has been suggested that MLC phosphorylation by MLC kinase is involved in the regulation of cardiac function (29, 30), and recent reports identified a novel heart-specific MLC kinase involved in the MLC phosphorylation (31, 32). Because the MLC phosphorylation is regulated by the bal-